A SCALABLE NON-LINEAR NOISE MODEL FOR HIGH-ELECTRON-MOBILITY TRANSISTORS

By

Vishal Kumar Sharma

A thesis submitted to Macquarie University

for the degree of Master of Research

Department of Engineering

April 2019

MACQUARIE
University
SYDNEY·AUSTRALIA

I, Vishal Kumar Sharma, declare that the work presented in this thesis is carried out at the Department of Engineering, Macquarie University, Sydney, Australia, between July, 2018 and April, 2019. To the best of my knowledge, the materials presented in this thesis, which are considered as thesis's novelty, are original and has not been submitted in whole or part for the degree in any other university or institution other than Macquarie University. The whole information obtained from other publications are all referred in the text and corresponding references are mentioned at the end of thesis.

Vishal Kumar Sharma

Acknowledgments

I would like to express my deepest and sincerest gratitude to my principal supervisor, Prof. Anthony Parker and my co-supervisor, Prof. Michael Heimlich, for their excellent support and quality supervision during this research work. I highly acknowledge their invaluable guidance and encouragement for successful and timely completion of this milestone.

I would also like to acknowledge Macquarie University for awarding me the Macquarie University Research Excellence Scholarship (iMQRES).

I would also like to acknowledge WIN Semiconductor Corporation for providing noise measurement data of 0.15μm enhancement-type GaAs-based p-HEMT.

I will always be grateful for the support and encouragement provided by the Prof. Simon Mahon, Gerry Mucculloch, and my colleagues in our research group especially, Dr. Sudipta Chakraborty, Dr. Bryan Schwitter, Dr. Oya Sevimli, Melissa Gorman and Irfan Shahid.

I will always be thankful to Prof. Keith Imrie and Prof. Simon Mahon, who provided a detailed edits of this thesis in a quick time.

I would also like to extend my regards to my wife Dr. Niharika Kohli who provide the grammar edits in my thesis in a quick time. She always encouraged me for working hard and thinking positively about the test problems.

Abstract

Noise is the unwanted random fluctuations in a signal, voltage or current. Over a frequency range from a few GHz to tens of GHz, the major noise contributors in the High-Electron-Mobility Transistor (HEMT) were thought to be partially correlated thermal drain-noise and gate-noise currents. However, the thermal origin of the drain-noise current cannot be explained with sub-micrometre HEMT theory. Furthermore, the measurements also reflect that both the noise figure and the optimum signal source admittance cannot be accurately defined using the conventional two noise sources. A simple but novel scalable non-linear noise model is presented in this thesis to predict the response and number of noise current sources in the HEMT in a frequency range from a few GHz to tens of GHz. The model uses probability theory, which is one of the best ways to predict the randomness associated with any quantity, for modelling noise in HEMTs, and describes how three noise sources are essential to completely define the noise performance of the HEMT over that frequency range. A comparison between the simulated and measured noise parameters is also carried out to test the validity of the model.

Contents

List of Figures

Chapter 1

Introduction

Over the last five decades, countless models have been developed to predict the characteristics of Field-Effect Transistors (FET). The need for high-speed and low-power consumption in electronic chips triggers down-scaling of the device dimensions, facilitated by advancements in device processing and the lithographic process. Due to this device scaling, second-order effects become significant in the device; for example the body effect, velocity saturation and the sub-threshold effect. Some of these effects and a few existing device characteristics under extreme bias conditions are difficult to predict using conventional device theory. One such extreme application is small-signal detection and amplification without degrading the original signal.

One of the major contributors that can contaminate the signal is the noise inside the device. Hence, to predict the degradation in the signal at the output of the circuit, one must first predict or model the noise generated in all the devices and parasitics involved in the circuit. Since the noise characteristics of a device are mainly determined by its noise parameters, the prime focus in noise modelling of the FET is to find a simple way to predict its noise parameters accurately. However, measurements of noise parameters are not only complicated but even harder to reproduce. The measurement data becomes further obscured due to variations in the noise performance of devices having identical dimensions but obtained from a different wafer lot. Furthermore, the physical origin of the noise sources in the FET is still ambiguous, which makes it difficult to predict over a wide range of frequencies and bias conditions. Such factors make noise modelling of the FET quite complex. Before understanding various possible noise sources and their origin, let us first briefly define the operation of the FET.

1.1 FET Operation

In general, a FET is a three-terminal device, where current flowing in the channel formed between the drain and the source terminals is controlled by the gate terminal. The FET is classified into three types: MOSFET (Metal-Oxide Field-Effect Transistor), MESFET (Metal Semiconductor Field-Effect Transistor) and HEMT (High-Electron-Mobility Transistor). For low-power and high-speed

applications, the latter two are well suited. Therefore, further discussion on noise modelling is focused on these two types of devices.

1.2 Noise in FETs

Noise is considered as unwanted random fluctuations in a signal, voltage or current. Although noise in an electronic circuit is due to many elements, the focus of this work is only on the noise generated by FETs (MESFET or HEMT). The origin of the noise inside the FET, over a wide range of frequency is from various mechanisms. Originally [1], noise in the FET was attributed to random fluctuations in the velocity of the charge carriers (electrons/holes) traversing the channel. These fluctuations in velocity are considered to be due to scattering of the carrier from thermally agitated lattice atoms, known as lattice scattering. These fluctuations are thought to be random because the small shift in the carrier velocity is random and independent among the carriers. Since the channel (drain) current is proportional to the carrier velocity, a random channel current is generated, termed a drain-noise current. Thus, the random channel current is the sum of a large number of tiny uncorrelated independent sources that are distributed uniformly across the channel [2]. At high frequencies, random fluctuations in the channel are coupled to the gate due to the capacitive coupling between the channel and the gate. This gate current is termed a gate-noise current [2, 3]. These drain-noise and gate-noise currents are partially correlated because they originate from the same sources within the FET. Since, thermal energy is responsible for carrier scattering, the spectral density of a noise source is assumed to be independent of frequency, thus it is Gaussian white noise. The equivalent noise circuit of an FET with two noise-current sources i_{ng} and i_{nd} [4] is shown in Figure 1.1.

Models of the thermal noise in the channel of a FET are based on models of the noise associated with a resistor [5, 6]. There are other non-thermal sources of noise that are significant at cryogenic temperatures inside an FET. These are independent of temperature [7]. At low frequencies, there is an additional noise source that is attributed to the gate leakage, which is shot noise. Initially it was thought to be an independent uncorrelated noise source [3]. However, a significant correlation is observed between the gate and drain noise currents as well [8]. Gate leakage can be assumed to be absent in the normal operation of an FET, although it can be significant in InP-based HEMTs [9].

Circuit designers characterise noise in terms of three fundamental noise parameters across frequency. These parameters are: minimum noise figure (NF_{min}), equivalent noise resistance (R_n) and optimum signal source admittance (Y_{opt}). These are often quoted on the device manufacturer's data sheets. Variation of these parameters with frequency is used by model designers to understand the nature of the noise sources in the FET. These parameters can be easily obtained using the noise theory of two-port networks after defining expressions for all the noise sources in the FET.

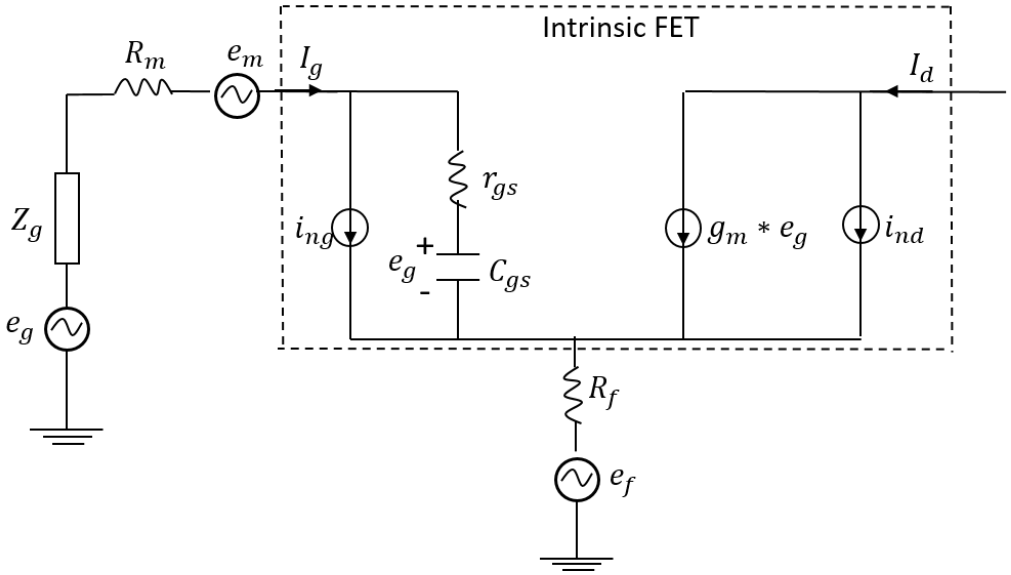

Figure 1.1: Small-signal noise equivalent representation of an FET with an input small-signal voltage e_g and a generator impedance Z_g [4]. The region inside the dotted line is the intrinsic FET with noise currents i_{ng} and i_{nd}. R_m and R_f are the parasitic gate and source resistances with corresponding noise voltage sources e_m and e_f.

1.3 Motivation and Objectives

The aim of this work is to identify the noise sources that are required to develop a non-linear noise model for an HEMT. It was found that the origin of the channel-noise current inside an HEMT cannot be considered as "thermal" in the sub-micrometre HEMT technology, the reason will be discussed in the subsequent chapters. Thus, a new approach is required to explain the origin of channel-noise current in the sub-micrometre HEMT technology. Since the noise is a random phenomenon, it can be described using a random variable which is a sum of many independent random variables. Thus, a probabilistic approach that can obtain a random variable, which can represents the randomness in the expected number of the charge carriers moving in the direction of the current inside the channel, can describe the channel-noise current. It is observed that the expression for spectral density of channel-noise current is similar to Schottky's theorem, in equation (2.35) of [10], since both are based on Poisson distribution of charge carriers:

$$\overline{i_d^2} = 2\,q\,I_d \tag{1.1}$$

This expression is also independent of frequency which is in conjunction with the results of past authors. The gate-noise current can also be considered as a result of the overall random fluctuations in the large number of channel charges which are coupled to the gate due to the capacitive coupling between the drain and gate of the FET, so it depends on the reactances of the C_{gd} (capacitance between drain and gate) and C_{gs} (capacitance between source and gate) and the voltage difference across the respective terminals. Hence, by defining noise statistically, one will be able to answer the

above-mentioned questions without the use of any assumptions. Also the model has the potential to deal with large signals, since it is not based on recording changes in noise current like previous models [1–3, 5]. Hence, a non-linear model can be developed using probability theory. Further discussion on the detailed theory will be presented in subsequent chapters.

The objective of the research activity is to develop a scalable non-linear model which can effectively describe the origin of all the noise sources and their correlation in the FET. The model should also evaluate fundamental noise parameters of the FET which are aligned with the measured data with minimum tolerance over a wide range of device geometry and bias points across a frequency range (mainly S band to K_a band). The selection of frequency range is driven by the need of noise model from the circuit designers, which were designing circuits in S to $\mathrm{K_a}$ band.

1.4 Synopsis

This dissertation is divided into five chapters starting with a pilot chapter to introduce the noise phenomenon in the FET and the need for the model. The last chapter describes the conclusion of the work stated in the thesis and the work that should be done in future. A brief overview of the remaining three chapters is given below:

Chapter 2 discusses in detail the theory for modelling "the noise" in FETs. Significant work carried out in the past regarding modelling noise in FETs is described, followed by their shortcomings in developing a noise model for sub-micrometre FETs. In the end, the challenges in noise modelling, which are primarily related to noise measurements, are discussed.

Chapter 3 describes the fundamental reason for the origin of the channel-noise current followed by detailed mathematics to support its stated origin. Thereafter, a new non-linear scalable noise model which is written in Verilog-A language and based on the said theory is described in the chapter using two noise-current sources. In the end, the need for another noise-current source, and a correction in the correlation between the discussed two noise currents, are deduced by comparing the analytical and measured noise parameters.

Chapter 4 describes both the new noise-current source and a correct correlation between the two noise-current sources. Afterwards, the noise model is revised based on three noise-current sources and is validated by comparing the analytical noise parameters with the measured results. Further, the model is also compared with the existing noise model developed by the WIN Semiconductor Corporation. Finally, to validate its functionality, it is integrated into the existing non-linear model, and a comparison between the S-parameters calculated using the integrated model and those obtained from measurements is given.

Chapter 2

Modelling Noise in FETs

The task of modelling noise in an FET over a frequency range from 2 GHz to 40 GHz can be divided into two sub-tasks. The first is to find expressions for the spectral density of the two prime partially correlated noise-current sources $\overline{i_{ng}^2}$ and $\overline{i_{nd}^2}$, and the second is to evaluate the fundamental noise parameters using the noise theory of a two-port network. Verification of the model is carried out by comparing the experimentally obtained noise parameters with the measured noise parameters across a wide range of frequencies, device geometries and bias points. These noise parameters can be obtained from the equivalent circuit of the intrinsic FET using two-port noise theory, which is discussed in the following section.

2.1 Theory of Noise in Two-Port Networks

An FET can be described as a linear two-port noisy network [11], in which all the noise sources are inside the network, as shown in Figure 2.1(a). This two-port noisy network is equivalent to a noiseless network with an additional voltage source at the input and output of the network as shown in Figure 2.1(b). An alternative representation is a noiseless network with an additional current source at the input and output of the network as shown in Figure 2.1(c), or a noiseless network with an additional voltage and current source at the input of the network as shown in Figure 2.1(d).

The network in Figure 2.1(c) is the best representation of the noisy FET among the three possibilities to model the total noise in FET using gate and drain noise currents which will be further explained in the subsequent chapters. The last network, in Figure 2.1(d), is the most widely used configuration as it reduces the complexity of solving the admittance or S-parameters of the network. Using two-port noise theory [11], the input-referred noise voltage (v) and noise current (i) in Figure 2.1(d) can be

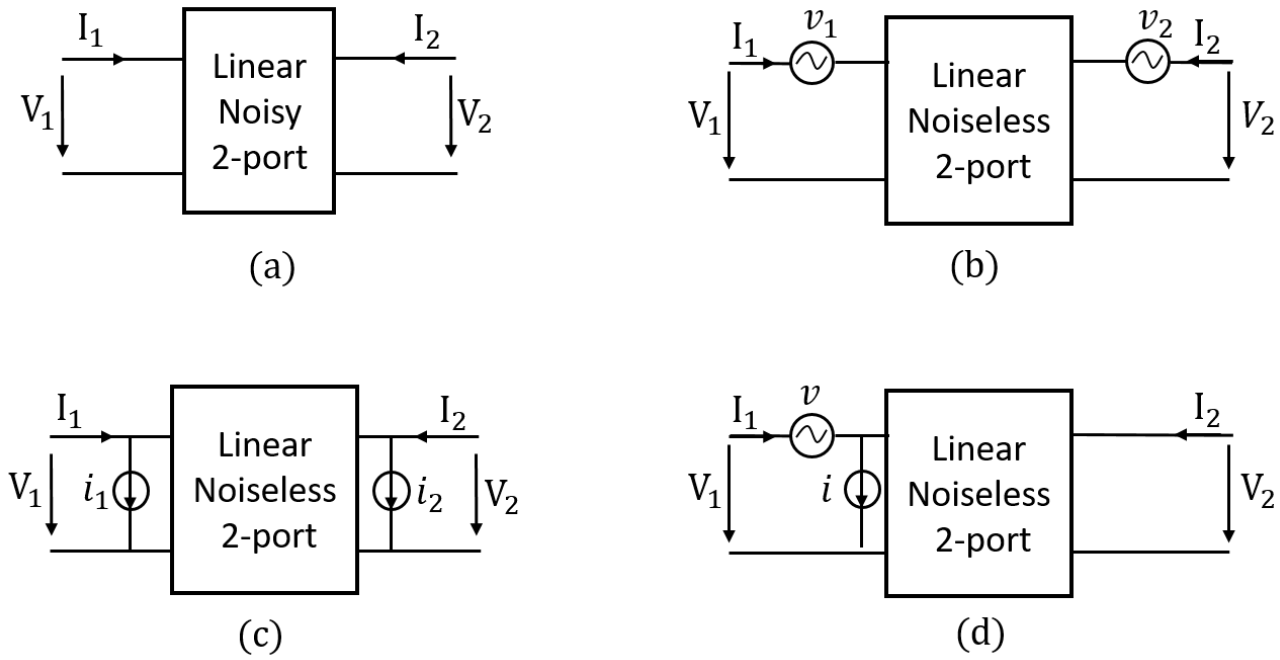

Figure 2.1: Noise representation in two-port network with: (a) Noise sources inside the network; (b) Noise current sources at input and output of noiseless network; (c) Noise voltage sources at input and output of noiseless network; (d) Noise current and voltage source at input of noiseless network [11]

.

described in terms of the two partially correlated noise-current sources (i_1 and i_2) in Figure 2.1(c) as:

$$v = -\frac{i_2}{Y_{21}} \tag{2.1}$$

$$i = i_1 - \left(\frac{Y_{11}}{Y_{21}}\right) i_2 \tag{2.2}$$

$$\overline{|v|^2} = -\frac{\overline{|i_2|^2}}{|Y_{21}|^2} \tag{2.3}$$

$$\overline{|i|^2} = \overline{|i_1|^2} - \left|\frac{Y_{11}}{Y_{21}}\right|^2 \overline{|i_2|^2} \tag{2.4}$$

where $\overline{|i_1|^2}$ = Spectral density of input noise current source (A^2/Hz)

$\overline{|i_2|^2}$ = Spectral density of output noise current source (A^2/Hz)

$\overline{|i|^2}$ = Spectral density of input-referred noise-current source (A^2/Hz)

$\overline{|v|^2}$ = Spectral density of input-referred noise-voltage source (V^2/Hz)

Since Y_{11} and Y_{21} are the matrix elements of the admittance parameter of the two-port noiseless network (an equivalent representation of the intrinsic FET), they can be obtained directly [4] using

Figure 1.1 as

$$Y_{11} = \frac{j\,\omega\,C_{gs}}{1 + j\,\omega\,C_{gs}\,r_{gs}} \tag{2.5}$$

$$Y_{21} = \frac{g_m}{1 + j\,\omega\,C_{gs}\,r_{gs}} \tag{2.6}$$

Since the noise-current sources (i_1 and i_2) are partially correlated with each other, the transformed noise sources (v and i) must also be partially correlated. The partial correlation can be defined by considering the noise-current source (i) to be composed of two current sources, one completely correlated to the voltage source (i_{cor}) and the other completely uncorrelated (i_{ucor}):

$$i_n = i_{cor} + i_{ucor} \tag{2.7}$$

These current sources can be expressed in terms of their associated noisy conductances such that

$$\overline{|i|^2} = 4\,k\,T_0\,G_n\,\Delta f \tag{2.8}$$

$$\overline{|i_{cor}|^2} = 4\,k\,T_0\,G_{cor}\,\Delta f \tag{2.9}$$

$$\overline{|i_{ucor}|^2} = 4\,k\,T_0\,G_{ucor}\,\Delta f \tag{2.10}$$

where k, T_0 and Δf are the Boltzmann constant, room temperature and frequency bandwidth, and G_n, G_{cor} and G_{ucor} are the respective noisy conductances.

The correlation coefficient (c) between the two noise sources (v and i) can be described using its basic definition as

$$c = \frac{\overline{i\,v^*}}{\sqrt{\overline{|i|^2}\,\overline{|v|^2}}} \tag{2.11}$$

Once the spectral density of the transformed noise sources (v and i) is obtained along with their correlation coefficient, the noise parameters: NF_{min}, R_n and Y_{opt} can be easily evaluated [4, 11] using the following expressions:

$$NF_{min} = 10\,\log_{10}[1 + 2\,R_n\,(G_{cor} + G_{opt})] \tag{2.12}$$

$$R_n = \frac{\overline{|v|^2}}{4\,k\,T_0\,\Delta f} \tag{2.13}$$

$$Y_{opt} = G_{opt} + jB_{opt} \tag{2.14}$$

$$\text{where} \qquad G_{opt} = \sqrt{\frac{G_{ucor}}{R_n} + G_{cor}^2} \tag{2.15}$$

$$B_{opt} = \Im\mathrm{m}\left\{\frac{\overline{i\,v^*}}{\overline{|v|^2}}\right\} \tag{2.16}$$

where, Y_{opt} is the optimum signal source admittance needed to reduce the noise figure of the FET to its minimum value. And G_{cor} and G_{ucor} are the respective noisy conductances of the correlated and uncorrelated part of input referred noise current.

Even though these fundamental parameters can define the randomness associated with the current flowing through the various terminals of the FET, they cannot predict the noise generated inside the device with respect to the 50 ohms input impedance. The noise inside the device corresponding to the 50 ohms input impedance can be represented by the parameter known as the noise figure (NF) which is defined by the ratio of the output noise to the input noise. However, this parameter can only be defined in terms of the fundamental noise parameters as

$$NF = NF_{min} + \frac{R_n}{G_s} |Y_s - Y_{opt}|^2 \tag{2.17}$$

$$\text{where} \quad Y_s = G_s + jB_s \text{ is the applied input signal impedance} \tag{2.18}$$

Thus, at a given frequency, equation (2.17) represents an ellipse in two dimensions, or a circle if $|G_s|$ and $|B_s|$ are equal. Therefore, the noise figure can be described as an ellipse as shown in Figure 2.2, centred at the minimum noise figure (NF_{min}), and the two axes of the ellipse are given by the real and imaginary parts of ($\frac{R_n}{G_s} |Y_s - Y_{opt}|^2$). If Y_s is equal to Y_{opt} then the circle will reduce down to a point where NF is equal to NF_{min}.

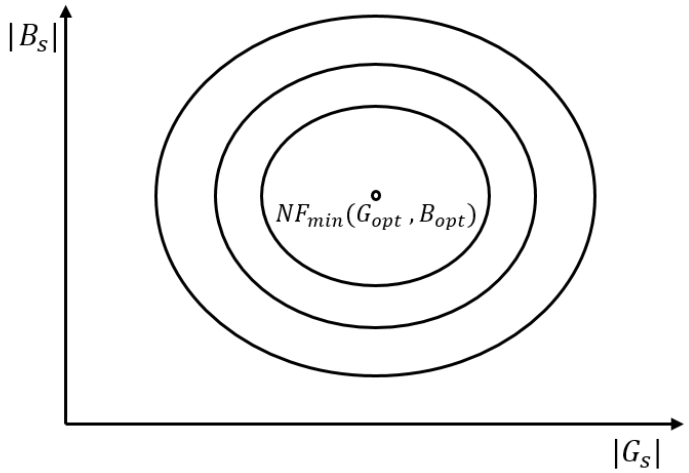

Figure 2.2: Noise-figure ellipse centred around minimum noise figure NF_{min}

Although the noise parameters can be easily obtained using noise theory, the applicabilities to FETs should be examined. The accuracy of the admittance parameters (in equation (2.5) and equation (2.6)) and their relations to the noise sources (equation (2.1) and equation (2.2)) should be reviewed. The spectral density of the two noise-current sources ($\overline{|i_1|^2}$ and $\overline{|i_2|^2}$) is assumed to be Gaussian, which should also be verified.

2.2 Intrinsic Admittance Parameters of FETs

The intrinsic admittance parameters of the FET are defined as the admittance parameters of the intrinsic FET (a FET without any parasitic element). The major problem in obtaining the intrinsic admittance parameters of the FET is that the intrinsic part of the FET is entirely enveloped inside the parasitic or access elements at the terminals of the FET [12] as shown in Figure 2.3. These parasitics present a significant impedances, especially at higher frequencies, and also vary with device dimensions. Hence, to obtain the intrinsic admittance parameters, a suitable experimental method [13] is required to subtract the admittance of these parasitic elements from the measured data (composed of intrinsic and parasitic admittance). The parasitic elements can be subtracted once their values are determined.

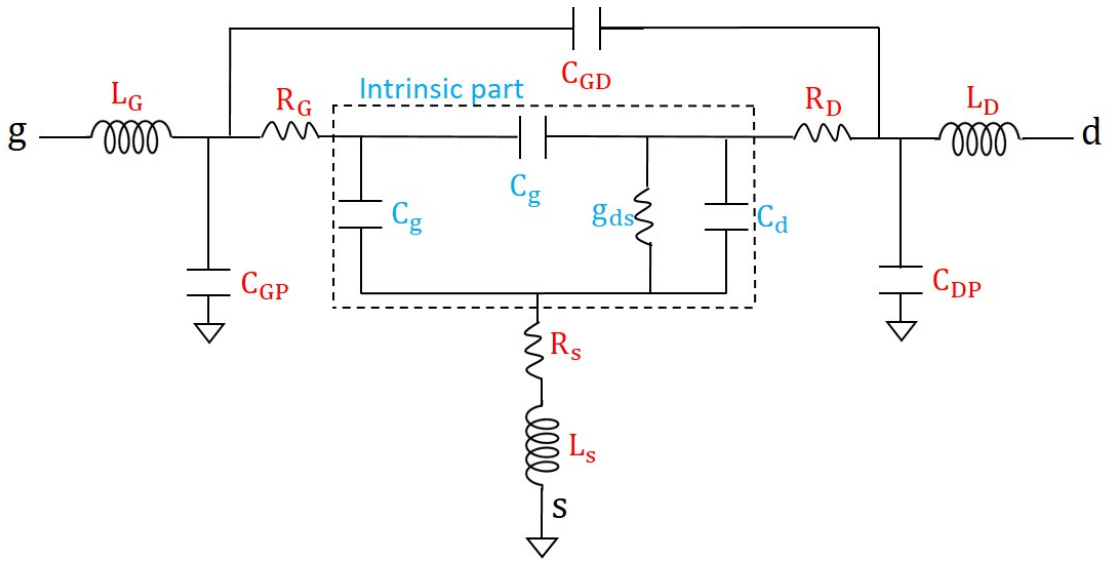

Figure 2.3: Small-signal equivalent circuit of FET [12] with zero drain bias, lateral channel symmetry and parasitic elements connected to its terminals

A common methodology to extract the parasitic elements is to bias the FET at zero drain voltage (also known as "cold FET condition"), and then compare the port parameters of the FET under the "ON" state and "OFF" states [13, 14] with the intrinsic circuit of the device [15]. However, it is observed that in the cold FET condition, the number of unknowns is more than the number of equations, hence the gate and the channel resistance of the FET must be assumed to be of some value at a certain gate bias, a priori [16, 17]. A priori gate and channel resistance can be estimated from their frequency response [12]. Thus, due to these prior assumptions, the final values of the intrinsic parameters are prone to uncertainty. Further, numerical techniques take long time to converge to the final value of the gate and channel resistance, and are also very tedious.

When describing the intrinsic part of the FET in terms of conductance and trans-capacitance as shown in Figure 2.4, it is possible to map the measured parameters (after subtracting the parasitic elements) directly with the admittance parameters of the intrinsic FET [12, 18]. This technique

provides a direct extraction.

The intrinsic small-signal FET model shown in Figure 2.4(b) can provide values of the admittance matrix that closely match the measured values over a wide range of frequency and hence can be considered reliable [12].

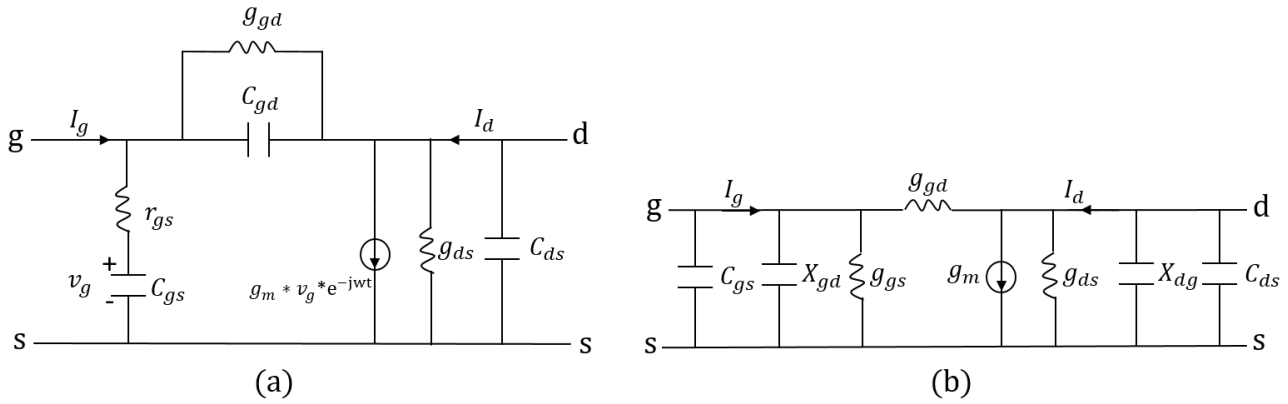

Figure 2.4: Equivalent circuit of intrinsic FET using: (a) time delay ($\exp(-jwt)$) and channel resistance r_{gs}, (b) trans-capacitance, for mapping of S-parameters [12]

2.3 High-Frequency Noise Sources in FETs

In this section, various noise sources that can impact the noise performance of the FET over the microwave frequency range (from S band to K_a band) are identified. Many models are able to predict the randomness in the channel and gate currents of the FET. The quest for the noise source(s) in the FET started with the first noise model [1] for the drain-noise current in 1962 by A. Van Der Ziel. In this model, the drain-noise current is considered to be of thermal origin and termed the thermal drain-noise current. Later on, the same author developed a model for the gate-noise current [3] as well. In the model, the gate-noise current is described with two noise sources; one is found to be partially correlated with the drain-noise current as both share the same thermal origin. The other is generated due to the gate leakage in the FET at low frequencies and termed the shot gate-noise current. The noise generation in the channel of an FET is considered to be due to the random fluctuations in the velocity of the charge carriers crossing the channel [19]. These velocity fluctuations were attributed to carrier scattering from thermally agitated lattice atoms. Both models were developed using the Shockley theory of the FET and hence were limited to long-channel FETs only.

H. Statz *et al.* developed a noise model [4] that is applicable to both short-channel and long-channel FETs (popularly known as PRC model). In this model, the channel of an FET is divided into two regions, such that in the first region the carrier velocity varies linearly with the electric field (constant mobility) and Shockley's principle applies. In the second region, an electron's velocity is saturated to a constant value in the presence of a high electric field. This model shares the same intuitions as Van

Der Ziel's on the origin of noise sources in FETs. Hence, the expressions of the spectral density of both noise-current sources in the two models only differ in their voltage-dependent parameters.

A. Cappy *et al.* used another approach to model noise in a sub-micrometre FET [2] such that the same approach can be used to model noise in HEMT devices as well [20]. The model was based on the theory of non-stationary electron dynamic effects, in which the drain-noise current is assumed to be a diffusion noise current rather than being thermal. Even though the approach was different from the H.Statz model, the expression for the noise-current sources in Cappy's model appears identical with the PRC model at low frequency. Also, the model is able to connect the noise parameters with the process parameters, thereby giving a way to find the noise performance of the FET without finding the noise sources. Later on, a noise source due to gate leakage at low frequencies in the FET [8] is also added to the model. Both gate-noise current sources are assumed to be partially correlated with their corresponding drain-noise current sources in this model.

Noise source modelling is complicated in the above analytical models. This is because of the various assumptions and experimental processes required for finding various theoretical fitting parameters. To avoid the complexity, a non-physical model [21] was developed by H. Fukui to relate the noise parameters directly to the process parameters. Although being simple, the model was still not able to fit across different FET technologies. The main limitation is that the fitting parameters can be determined only after Noise Figure determination. Also, the fitting parameters vary with device geometry. Therefore, fitting parameters have to be determined for each device geometry.

M. W. Pospiezalski developed a two-parameter noise model [6, 22]. In this model, the channel-noise current is considered to be due to the trans-conductance (g_m) and is represented by the spectral density of drain-noise current ($\overline{i_d^2}$), and the gate-noise current was considered to be due to the input gate resistance (r_{gs}) and is represented by the spectral density of the gate-noise voltage ($\overline{v_g^2}$).

$$\overline{i_d^2} = 4\,k\,T_d\,g_m \tag{2.19}$$

$$\overline{v_g^2} = 4\,k\,T_g\,r_{gs} \tag{2.20}$$

Although both sources are presented as independent of each other [23], they were defined in the model as partially correlated. Thus, the model uses only two frequency-invariant parameters T_d and T_g termed noise temperatures, to describe the noise performance of the FET. Furthermore, the model was applicable for any type of FET including MOSFETs [24]. A typical value of the noise temperature T_d is in the range of 5460 K to 5520 K for g_m of 3.24 mS to 3.27 mS [6]. However, the noise temperature T_g is calculated to be around 210 K to 310 K, which is close to room temperature for r_{gs} in the range of 2.5 Ω to 3.5 Ω [6]. These values of the noise temperature are obtained at the same bias condition, V_{ds} being at 2 V to provide a drain current (I_{ds}) of 10 mA. The value of the electric field between the drain and gate terminals is difficult to predict as the gate voltage is not provided in the reference.

Although the expression for the spectral density of the noise current (or voltage source) and calculation of the fundamental noise parameters are quite straightforward in the model, the accuracy of the noise model depends completely on the merits of the extraction process of the two linear FET parameters, g_m and r_{gs}.

The desire to reduce the number of fitting parameters led to the setting of the noise temperature T_g to the room temperature [25]. However, this assumption drastically reduces the accuracy of the model, as there is no criterion in this situation to counterbalance the inaccuracies generated in the extraction of the parameter r_{gs}. This confirms that at least two degrees of freedom are necessary to predict the noise performance of the FET in the microwave frequency range.

Recent literature [26, 27] shows that both the PRC model and an equivalent noise model can predict a similar noise performance for both GaAs and GaN based HEMTs for small-signal applications. However, the equivalent noise model uses one degree of freedom less in the noise-performance prediction. This looks advantageous [28], however, the methodology is found to be less effective in large-signal applications [27]. The ineffectiveness of the model is the result of the principal problem that exists between large-signal and small-signal FET parameters, as the small-signal FET parameter g_{ds} (used in the noise-temperature equivalent model) is not equal to the drain-current derivative $G_{ds} = \dfrac{\partial I_{ds}}{\partial V_{ds}}$. Hence, the drain-noise current is found to be different in the two applications. Moreover, the initial assumptions used in the equivalent noise model for R_{gs} further lower its efficiency for large-signal applications.

Another important point on the noise source was discussed in recent literature [7] for a cryogenic temperature range. It had been observed that the drain-noise current does not posses any thermal origin. However, the gate-noise current is proportional to T_g. This clearly shows that the gate-noise current is completely independent of the drain-noise current. However, it should be noted that this statement is only in reference to cryogenic temperatures.

After going through a brief but fruitful discussion on the noise phenomenon inside the FET under various conditions, it becomes necessary to summarize the key points about noise sources in the FET,

- The prime noise sources needed to predict the noise performance in FETs which are unanimously accepted in all models are:
  - Partially correlated drain and gate noise.
  - A gate-noise source associated with the gate leakage current. However it is limited to InP-based HEMTs, since the gate leakage is negligible in other HEMTs.
- The origin of the drain-noise current in the FET is considered to be thermal in all models except at cryogenic temperatures. However, the thermal origin of the drain-noise current cannot be explained with the sub-micrometre HEMT device theory.

- Because of the randomness involved with the noise performance of the device, none of the above models are able to provide a simple way to predict and verify the noise performance of the FET.
- At least two parameters are necessary to describe the partially correlated noise sources in the FET.
- Apart from the PRC model no other model is able to make an accurate prediction of the noise performance of the HEMT under large-signal applications.
- Noise modelling using an empirical method is found to be more tedious and less reliable than an analytical method.
- No model has discussed the impacts of parasitics on the noise performance of the FET.

2.4 Challenges

Developing a noise model for the FET has been a challenge, as the root cause of the noise generation in the FET is still ambiguous. The prime challenges in the noise modelling can be summarised as follows:

- Making an accurate prediction of the randomness associated with the current flowing across various terminals in the FET is difficult. The coefficient associated with the spectral density of noise sources is calculated from the response of measured noise parameters with frequency. Therefore, any inappropriate coefficient value makes it difficult to guess whether the measured data is wrong or the model is incorrect. A small variance either in the prediction or in the measurement can result in non-physical noise parameters of the device. This can either shift the centre of the Noise Figure ellipse or deform its shape.
- Measuring noise parameters accurately is also quite difficult. Since, the noise-power spectral density is very small, recording an accurate reading is a challenge because of the following constraints [29]:
  - The excessive Noise Ratio (ENR) of the noise source must be comparable to the noise figure (NF) of the device under test (DUT). A smaller ENR of the noise source than the noise figure of the DUT will result in an error.
  - Maintaining a low-loss path between the noise source and the DUT, besides attaining a good match between each neighbouring component, is a challenge.
  - The noise figure of the mixer which provides sufficient down conversion in frequency must be a minimum to keep the system's ENR lower than the NF of the DUT.

  - Insertion losses must be a minimum in the section between the impedance tuner and the DUT. Otherwise, this can shift the optimum signal source admittance (Y_{opt}).
  - Apart from a low noise figure of the system, one must also ensure that the dynamic range of the entire signal is not very high, otherwise the signal would get saturated or clipped at some stage.

- The admittance parameter of the intrinsic FET must not change during the noise-parameter measurements i.e, all parasitic elements must be removed before starting the measurements. Otherwise, this would change the spectral density of the noise current sources and then the noise parameters.

Chapter 3

Noise Model Based on Charge Fluctuations

This chapter describes a fundamental model for the origin of the drain-noise current in the HEMT and how it is different from past intuition. This is followed by the detailed mathematics that supports the discussed prediction on the origin of the drain-noise current. Using this theory, a new noise model and its implementation using Verilog-A code is described to predict the noise performance of the HEMT. Thereafter, the response of the measured fundamental noise parameters with various device geometries and bias points over the frequency range from 2 GHz to 40 GHz are reported to provide noise model to the circuit designers developing designs in S to $\mathrm{K_a}$ band. In the end, the results of the new model are discussed and compared with the measured results.

3.1 Origin of Drain-Noise Current in HEMT

The advancements in HEMT technology over the past two decades have resulted in a continuous decrease in both the gate length (an overlap region between gate metal and depletion layer) and the channel length (a separation between the source and drain contacts) of the sub-micrometre HEMT [30–33]. One of the prime aims of this reduction was to capitalise on the velocity overshoot effect related to the velocity of the charge carriers present in the channel of the sub-micrometre HEMT [34, 35]. This effect results in a drastic increase in their velocity under suitable drain and gate voltages [36]. With these improvements, the charge carriers can traverse the complete channel primarily at their peak velocity (enhanced by the velocity overshoot effect). As a result of the high velocity, the mean path-length of a charge carrier's scattering has become larger than the gate length [equal to or lower than 0.15 μm] in the present-day sub-micrometre HEMT technologies [36]. These numbers indicate that most of the charge carriers come out of the channel before getting scattered by the thermally agitated lattice atoms. Hence, in the present sub-micrometre HEMT technology, the origin of the drain-noise current inside an HEMT cannot be considered as "thermal".

Now, the question arises "what could be the source of the noise in the channel?" One possible cause of the channel-noise current could be the random fluctuations in the large number of charge carriers contributing to the channel current. These random fluctuations in the large number of charge carriers arise because of the uncertainty in predicting their position and momentum simultaneously due to their high speed.

However, these random fluctuations can be anticipated if the large number of charge carriers crossing the channel per unit time are observed in small time slots for a long duration. This provides the time distribution of the fluctuations in the number of charge carriers reaching the drain terminal per unit time. Then the average number of fluctuations in the number of charge carriers crossing the channel per unit time can be evaluated from the distribution and the spectral density of those random fluctuations can be calculated.

3.2 Spectral Density of a Noise Current

The spectral density of a random variable, which describes a random process constituting a large number of small random independent events, can be defined using Schottky's theorem if the process obeys a Poisson distribution. The noise current generated due to the random fluctuations in the large number of charge carriers can be considered as one such random process.

3.2.1 Drain-Noise Current: A Random Process

Consider a large number of charge carriers traversing the channel region between the source and drain terminals of the HEMT under a positive potential difference. The charge carriers arriving at the destination (drain) terminal in a small time τ can be considered as one tiny random event, with an outcome being the number of charge carriers arriving at the destination terminal per unit time. Let these random independent events be observed over a large time interval, $0 \leq t \leq T$, i.e. T tends to infinity. It can be assumed that after this interval the whole process will repeat itself and the periodicity of every random event involved in this process will be equal to T.

Let the probability density ($g_\tau(\tau)$) of an event in time duration τ be defined as its number of occurrences divided by the total number of events in the sample space. Then, the probability of this event in the time duration τ is given as $g_\tau(\tau).\tau$. Also, it should be noted that the total probability of all such events must be one.

$$\int_0^\infty g_\tau(\tau) d\tau = 1 \tag{3.1}$$

Let the random independent events occur at an average rate λ (average of the number of charge

carriers arriving at the drain terminal per unit time). Hence, for an average drain current I,

$$\lambda = \frac{I}{q} \tag{3.2}$$

Therefore, the approximate number of events occurring in time T, will be λT.

3.2.2 Spectral Density of Fluctuating Charge Carriers

Consider a random variable $X(t)$ that constitutes the randomness in the process which is comprised of the above independent events ($X_i(t)$). Hence, the random variable $X(t)$ will be the sum of the outcomes ($X_i(t-t_i)$) of each independent event which starts at the time instant t_i

$$X(t) = \sum_i X_i(t-t_i) \tag{3.3}$$

These outcomes are completely integrable in the time domain. Furthermore, the events are considered to be memoryless, such that the information about the outcome of a past event cannot influence the outcome of future events. Therefore, the outcome of any independent event starting at any instant t_i will be considered as zero for $t < t_i$:

$$X_i(t-t_i) = 0 \quad \text{for } t < t_i \tag{3.4}$$

Let's consider an i^{th} random event $X_i(t)$ starting approximately at the middle of the random process, that is $t_i \approx \frac{T}{2}$. The Fourier coefficient associated with the outcome ($X_i(t-t_i)$) of the i^{th} random event is given as

$$a_n = \frac{1}{T}\int_0^T X_i(t-t_i)\exp(-j\omega_n t)\,dt \tag{3.5}$$

Changing the variable from t to u ($u = t - t_i$) and assuming that T tends to infinity, we get

$$a_n = \frac{\exp(-j\omega_n t_i)}{T}\int_{-\infty}^{\infty} X_i(u)\exp(-j\omega_n u)\,du \tag{3.6}$$

Since the Fourier transform of any function $F(t)$ can be given as

$$\Psi(f_n) = \int_{-\infty}^{\infty} F(t)\exp(-j\omega_n t)\,dt \tag{3.7}$$

The Fourier coefficient for the outcome of an i^{th} random independent event is given as

$$a_n = \frac{\exp(-j\omega_n t_i)}{T}\Psi_i(f_n) \tag{3.8}$$

Using the Wiener-Khintchine theorem [37], the spectral density of the outcome of an i^{th} random independent event for sufficiently large T is represented as:

$$S_i(f_n) = \lim_{T\to\infty} 2\,T\,a_n\,a_n^* \tag{3.9}$$

$$S_i(f_n) = \frac{2|\Psi_i(f_n)|^2}{T} \tag{3.10}$$

where a_n^* is the complex conjugate of the Fourier coefficient a_n.

Thus, the spectral density of a random variable $X(t)$ constituting approximately λT events can be given as

$$S_x(f) = \lambda\,T\,\overline{S_i(f)} \tag{3.11}$$

where, $\overline{S_i(f)}$ represents the average of the spectral densities of the outcome of the i^{th} random independent event over a sufficiently large frequency spectrum. Thus, subscript n is removed in the equation. Using equation (3.10),

$$S_x(f) = 2\,\lambda\,\overline{|\Psi_i(f)|^2} \tag{3.12}$$

where $\overline{|\Psi_i(f)|^2}$ represents the average of the square of the absolute value of all random frequency samples for an outcome of the i^{th} random independent event over the frequency spectrum. In other terms, it represents the auto-correlation of the random variable $X_i(t)$ over the time duration τ. Using the definition of the expectation value of any random variable $|\Psi_i(f_n)|^2$ with a probability density function $g_\tau(\tau)$ we get

$$\overline{|\Psi_i(f)|^2} = \int_0^\infty |\Psi_i(f_n)|^2\,g_\tau(\tau)d\tau \tag{3.13}$$

Thus, equation (3.12) will be given as

$$S_x(f) = 2\,\lambda \int_0^\infty |\Psi_i(f_n)|^2\,g_\tau(\tau)d\tau \tag{3.14}$$

Using the result of the Wiener-Khintchine theorem ($|\Psi(0)| = q$) and equations (3.1)-(3.2), the spectral density of the random variable $X(t)$ will be given as

$$S_x(0) = 2\,q\,I \tag{3.15}$$

Thus, the total variance in the current flowing between two terminals, will be given by 2q. In other words, equation (3.15) represents the spectral density of the noise current which is attributed to a large number of random independent events with an average occurrence rate of λ. This result is similar to **Schottky's theorem**. However, Schottky's theorem describes the random fluctuations in the number of electrons emitted from a thermionic saturated cathode.

The spectral density of the noise current is independent of the frequency (from equation (3.15)). Hence, it can be considered as a Gaussian (white) noise. This is in sync with the probability theorem, which states that the distribution of any random process comprising of large number of small random independent events will be a Gaussian irrespective of the distributions of the small independent events.

The spectral density of the random number of charge carriers arriving at the drain terminal per unit time can be obtained as follows:

$$I = q\,\overline{n} \tag{3.16}$$

$$\text{or,} \quad \overline{n} = \frac{I}{q} \tag{3.17}$$

$$\text{and} \quad d\overline{n} = \frac{dI}{q} \tag{3.18}$$

where $\overline{n}$ is the average number of charge carriers arriving at the drain terminal per unit time.

The spectral density of the current $S_x(0)$ and the number of charge carriers per unit time $S_n(0)$ can be related to each other using equation (3.17) as

$$S_n(0) = \frac{S_x(0)}{q^2} \tag{3.19}$$

Using equation (3.15),

$$S_n(0) = 2\,\overline{n} \tag{3.20}$$

With the expression of noise spectral density (equations (3.15) and (3.20)), a new noise model for the FET can be developed using the correlated noise sources.

3.3 Correlated Noise Sources in a HEMT

As discussed in Section 3.2.1, the random fluctuations in the number of charge carriers crossing the region between the two terminals of the HEMT per unit time constitutes the noise current flowing between those two terminals. Thus, the spectral density of the drain-noise current or variance of current per hertz of bandwidth $[\mathrm{A}^2/\mathrm{Hz}]$ can be defined using equation (3.15) as

$$\frac{\overline{i_{nd}^2}}{\Delta f} = 2\,q\,N_{ds}\,I_{ds} \tag{3.21}$$

where i_{nd}, I_{ds} and N_{ds} represent the drain-noise current, the dc drain current and the drain-noise coefficient, respectively.

In a practical situation it is difficult to verify whether all the random fluctuations in the number of charge carriers generated across the channel per unit time are able to reach the drain terminal. Hence,

a scalar factor N_{ds} is used in equation (3.21). The drain-noise current [A] is given as

$$i_{nd} = \sqrt{2\, N_{ds}\, q\, I_{ds}\, \Delta f} \tag{3.22}$$

At high frequencies, the random fluctuations in the number of charge carriers present in the channel coupled to the gate depending on the reactance of C_{gd} (capacitance between the drain and gate terminals) and C_{gs} (capacitance between the source and gate terminals) and the noise voltage developed in the channel. Let N_{cc} be the number of charge carriers that are being coupled to the gate terminal in time τ, so the coupled charge will be $q_{cc}\,(= q\, N_{cc})$. The charge spectral density [C^2/Hz] of the overall random fluctuations in the coupled charge (q_{ncc}) can be expressed in terms of the spectral density of the overall fluctuating number of coupled charge carriers at an instant of time τ using equation (3.20) as

$$\frac{\overline{q_{ncc}^2}}{\Delta f} = q^2\, 2\, \overline{N_{cc}} \tag{3.23}$$

$$\frac{\overline{q_{ncc}^2}}{\Delta f} = 2\, q\, \overline{q_{cc}} \tag{3.24}$$

where $\overline{q_{cc}}$ [C/Hz] represents the charge associated with the average of the coupled charge carriers ($\overline{N_{cc}} = \overline{n_{cc}}\,\tau$) in time τ.

Since in short channel devices, electric field along the channel cannot be neglected and hence must be considered to distribute the channel charge along the source and drain side of the gate region [38]. Thus, the random fluctuations in the coupled charge from source and drain side of the gate region must also be partitioned using the same principle. Therefore, the overall random fluctuations in the coupled charge must be represented as the weighted sum of the source and drain side coupled fluctuating charges such that

$$q_{ncc} = q_{ngd}\left(\frac{\overline{q_{ngd}^2}}{\overline{q_{ncc}^2}}\right) + q_{ngs}\left(\frac{\overline{q_{ngs}^2}}{\overline{q_{ncc}^2}}\right) \tag{3.25}$$

where $\overline{q_{ngd}^2}$ and $\overline{q_{ngs}^2}$ represent the charge spectral density [C^2/Hz] of the fluctuating coupled charge under the drain and source sides of the gate.

Thus, the spectral density of the coupled charge under the drain and source sides of the gate can be expressed using equation (3.24) as

$$\frac{\overline{q_{ngd}^2}}{\Delta f} = 2\, q\, \overline{q_{cc}}\, \gamma_{sd} \tag{3.26}$$

$$\frac{\overline{q_{ngs}^2}}{\Delta f} = 2\, q\, \overline{q_{cc}}\, (1 - \gamma_{sd}) \tag{3.27}$$

where γ_{sd} is a scalar charge-distribution factor in the range of $0 \leqslant \gamma_{sd} \leqslant 1$.

The total gate-noise current [A] associated with the overall random fluctuations in the coupled charge is given as [3]

$$i_{ng}(\omega) = j\,\omega\,(q_{ncc}) \tag{3.28}$$

$$i_{ng}(\omega) = j\,\omega\,\sqrt{2\,q\,\overline{q_{cc}}\,\Delta f} \tag{3.29}$$

Hence, the spectral density of the total gate-noise current [$\mathrm{A^2/Hz}$] will be given as

$$\frac{\overline{i_{ng}^2}}{\Delta f} = 2\,\omega^2\,q\,\overline{q_{cc}} \tag{3.30}$$

Since both the gate-noise and drain-noise currents are generated from the same source, they must be correlated (partial or complete). Consequently, the cross-covariance between the two noise sources is given as

$$\overline{q_{ncc}^*\,i_{nd}} = 2\,q\,\Delta f\,\sqrt{N_{ds}\,\overline{q_{cc}}\,I_{ds}} \tag{3.31}$$

$$\overline{i_{ng}^*\,i_{nd}} = -\,j\,\omega\,2\,q\,\Delta f\,\sqrt{N_{ds}\,\overline{q_{cc}}\,I_{ds}} \tag{3.32}$$

where q_{ncc}^* and i_{ng}^* are the complex conjugates of the overall random fluctuations in the coupled charge and the gate-noise current, respectively.

Since both I_{ds} and $\overline{q_{cc}}$ are functions of the gate and drain voltages and the device geometry, the drain and gate noise currents can be calculated for any bias point and device geometry at any high frequency using the equations (3.22) and (3.29), which will be shown in section 4.4 in the next chapter.

The required expressions of the spectral density of the correlated noise sources and their cross-covariance are thus obtained. Although, the spectral density of the drain-noise current is independent of the frequency (equation (3.21)), the spectral density of the correlated gate-noise current is a function of frequency (equation (3.30)).

There are two unknowns, N_{ds} and $\overline{q_{cc}}$, in the spectral-density expressions (equations (3.21) and (3.30)) of the correlated noise currents. The values of these unknowns can be determined by relating the analytical noise parameters to the measured noise parameters. Thus, a scalable noise model across various device geometries in the Verilog-A language can be developed using the above expressions of correlated noise currents.

The analytical expressions of both noise sources are of the same nature as those predicted by past authors, however the expressions are much simpler than the previously published expressions, with fewer unknowns to calculate from the measured data. Hence, the model is less likely to produce non-physical results.

3.4 Verilog-A Implementation of the Noise Model

Verilog-A has emerged as a preferred language for writing compact models [39]. The Verilog-A language has built-in functions to implement noise sources in electrical circuits. Furthermore, most of the current simulators including harmonic balance use verilog-A code in simulating semiconductor device models. Hence, the noise model is developed in Verilog-A language. A white-noise source with a given spectral density can be described using the Verilog-A function "white_noise (Var)" where Var represents the variance in the white-noise source. Each "white_noise ()" function generates a unique noise source which could be either a voltage, current or charge noise source, which is completely uncorrelated to any other noise source generated by it even with the same spectral density [40]. As discussed in Section 3.3, both the gate-noise current and the drain-noise current are generated from the common source "random fluctuations in the channel charge" and thus are correlated. Hence, the correlated noise sources must be implemented using a single "white_noise ()" function.

The variance in the overall channel charge due to the random fluctuations in the charge carriers arriving at the drain terminal per unit time is given as 2q, as described in equation (3.15). A white-noise source with a variance 2q in the Verilog-A language is described as

$$\sigma = white\_noise(2q)\,; \tag{3.33}$$

The drain-noise current [$\mathrm{A}/\sqrt{\mathrm{Hz}}$] and noisy coupled charge [$\mathrm{C}/\sqrt{\mathrm{Hz}}$] can be described using equations (3.22), (3.26) and (3.27) in the Verilog-A language as:

$$i_{nd} = \sigma\,\sqrt{N_{ds}\,I_{ds}}\,; \tag{3.34}$$

$$q_{ngd} = \sigma\,\sqrt{\overline{q_{cc}}\gamma_{sd}}\,; \tag{3.35}$$

$$q_{ngs} = \sigma\,\sqrt{\overline{q_{cc}}(1-\gamma_{sd})}\,; \tag{3.36}$$

In Verilog-A language, a $ddt()$ operator is used to implement the $j\omega$ term in the expressions of gate-noise current and the cross-variance of two noise sources. Thus, the terminal drain-noise current [$\mathrm{A}/\sqrt{\mathrm{Hz}}$] and gate-noise current [$\mathrm{A}/\sqrt{\mathrm{Hz}}$] can be obtained by adding the drain-noise current and the noisy charge into their corresponding terminal currents.

$$I(d,s) <+ \sigma\,\sqrt{N_{ds}\,I_{ds}}\,; \tag{3.37}$$

$$I(g,d) <+ \sqrt{\overline{q_{cc}}\gamma_{sd}}\,ddt\{\sigma\}\,; \tag{3.38}$$

$$I(g,s) <+ \sqrt{\overline{q_{cc}}(1-\gamma_{sd})}\,ddt\{\sigma\}\,; \tag{3.39}$$

where the $<+$ operator is used to add an expression to the existing value of a terminal current or voltage.

3.5 Analysis of Measured Data

The first step in the compact modelling is to validate the measured data and to rectify all the incorrect data points. Otherwise, the model can lead to non-physical results. There are several factors, as discussed in Section 2.4, that can cause a incorrect noise measurement. Hence, the measured data points which are not following the trend are not considered in validating the noise model. The analysis of the measured data also helps in understanding the response of the noise sources with the device geometry, bias points and frequency.

The noise measurements were carried out by the research and development (R&D) team in the industry "WIN Semiconductor Corporation". The HEMTs used in the measurements are products of the $0.15\,\mu\mathrm{m}$ enhancement-type GaAs-based p-HEMT technology. The number $0.15\,\mu\mathrm{m}$ refers to the gate length of the HEMT, and the word p-HEMT refers to the pseudomorphic HEMT, i.e, a HEMT in which the thin channel layer (GaAs layer) is strained in order to provide a lattice match at the interface between the two different-bandgap semiconductor materials (GaAs and AlGaAs in this case) [41].

A brief description of the device geometries and bias points used in the measurement is as follows:

- The measurements were done over a wide range of most commercially used device geometries to cover all possible extreme combinations. The devices used in the measurements are $\mathbf{25\,\mu m, 50\,\mu m \text{ and } 75\,\mu m}$ wide, with three different possible number of gate fingers $\mathbf{2, 4 \text{ and } 8}$. Hence, a total of **nine** devices are used in the measurements.

- The measurements were carried out at five different bias points. Each device, which is biased at a fixed drain voltage (V_{ds}), is subjected to five different gate voltages (V_{gs}) to conduct a corresponding five different drain currents ranging from **50 mA/mm** to **250 mA/mm** in steps of **50 mA/mm**.

- The noise performance of the HEMT for all device geometries and bias points is measured over **2 GHz** to **40 GHz**, covering both the S band and the $\mathrm{K_a}$ bands of microwave frequency.

- All the HEMT devices that were used in the measurements were fabricated on the same wafer. Further, none of the measurements are repeated on any other device with the same dimensions or bias point due to the small time frame of six months and resource constraints. Hence, the reproducibility of the measurement is not validated.

The three fundamental noise parameters (NF_{min}, Y_{opt} and R_n) along with the noise figure (NF) of the intrinsic HEMT device were measured for all the discussed device geometries and bias points over the mentioned frequency range. The S-parameters of the intrinsic HEMT are also measured across all the discussed possible configurations to ensure that no additional parasitic elements have been

added across the HEMT during the measurements, which can corrupt its noise performance. The validation for the presence of the parasitic elements during the noise measurements can be done by comparing the S-parameters measured during the device characterisation [12] and during the noise measurements.

After understanding all the possible input device geometries and bias points along with the measured output noise parameters required for the detailed investigation of noise in the HEMT, the focus of this section is to build further knowledge about the nature of the noise currents in the device and to identify the false measured data points.

3.5.1 Speculation on the Nature of Noise Currents from Measured Data

The response of the minimum noise figure (NF_{min}) with various device geometries and drain currents can highlight various features of the noise sources in the HEMT. Hence, it can be used to verify the number and the behaviour of the noise sources required to predict the noise performance of the HEMT. A brief description of the behaviour of the minimum noise figure (NF_{min}) and corresponding hypothesis on the noise current across the mentioned frequency range for various device geometries and bias points is as follows:

- The Minimum noise figure increases with an increase in the device width at any frequency point as shown in Figure 3.1(a) and 3.1(b). This response was expected, as the channel-noise current is proportional to the square root of the drain current or the device width.

- The minimum noise figure is observed to remain constant or be marginally reduced with an increase in the number of gate fingers at any frequency point as shown in Figure 3.2(a) and 3.2(b). Each finger corresponds to one channel and one gate, which generates a pair of noise currents (being correlated). Hence, the number of gate fingers is proportional to the correlated noise currents. However, the correlated noise currents associated with each finger are uncorrelated among the gate fingers. Hence, the randomness in the charge among different fingers may cancel each other, as the electric field across each channel is the same.

- The minimum noise figure also increases with an increase in the frequency in the said frequency range for any given device geometry, as shown in Figure 3.3(a). This behaviour is quite critical, as only the gate-noise current is proportional to the frequency (equation (3.29)) and has a lower magnitude than the drain-noise current, being proportional to the average of the number of fluctuating charge while the drain-noise current is a function of the dc drain current. Hence, it will be interesting to analyse whether an additional noise source is required or whether the spectral density of the gate-noise current can validate the behaviour.

- The minimum noise figure also keeps on increasing with an increase in the dc drain current at any given frequency as shown in Figure 3.3(b), as expected from the noise-current expressions

(equation (3.22) and equation (3.29)).

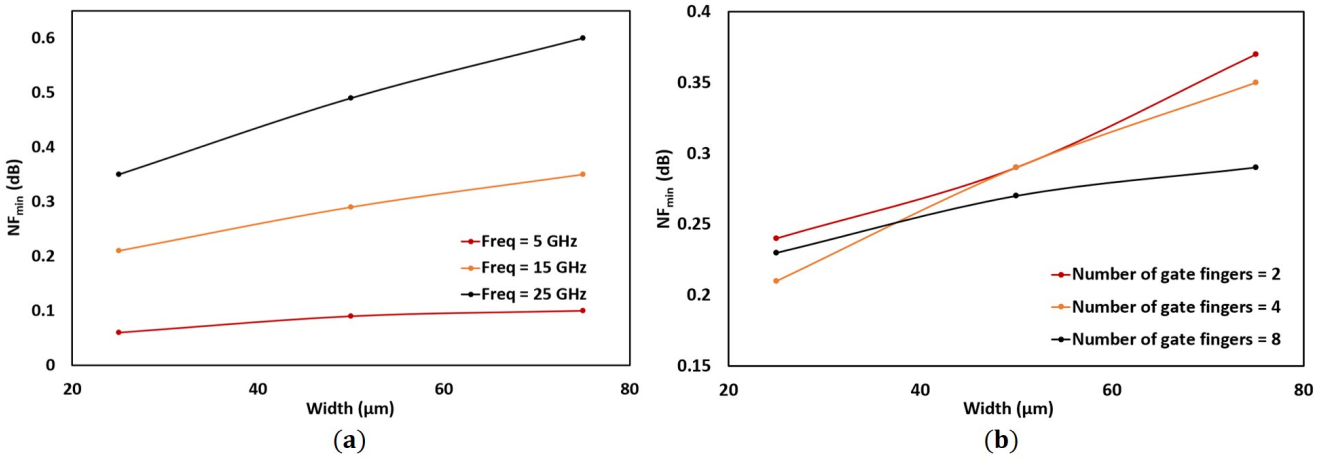

Figure 3.1: Response of measured NF_{min} across various device widths biased to conduct a drain current (I_{ds}) of 100 mA/mm: (a) For three different frequencies with number of gate fingers = 4 (b) For three different numbers of gate fingers at frequency 15 GHz

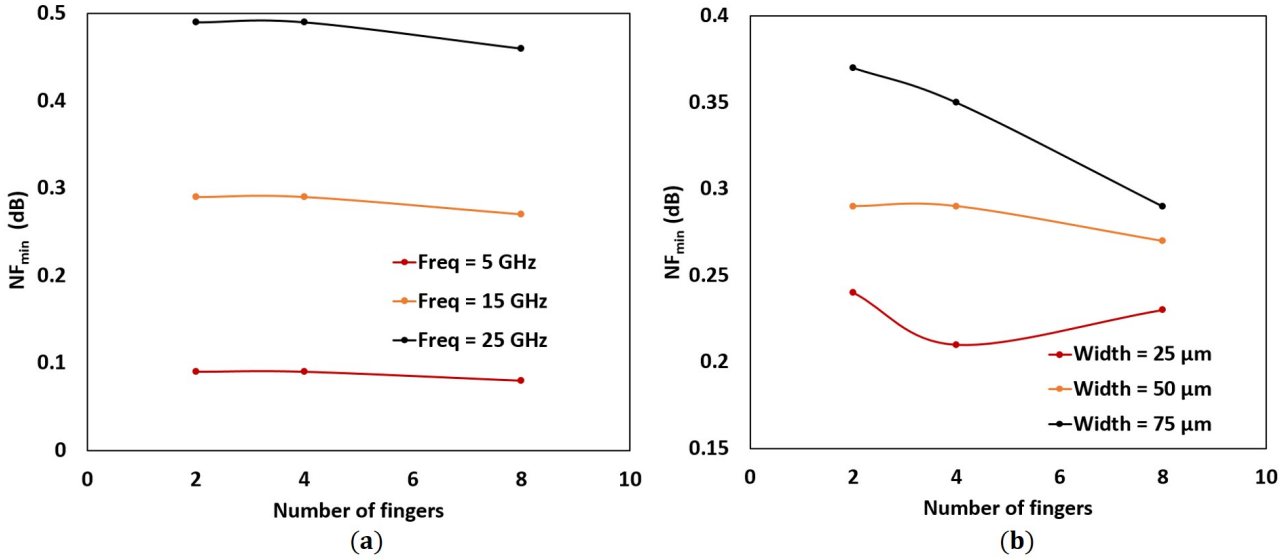

Figure 3.2: Response of measured NF_{min} across various numbers of gate fingers, biased to conduct a drain current (I_{ds}) of 100 mA/mm: (a) For three different frequencies with device width = 50 μm (b) For three different device widths at frequency 15 GHz

3.5.2 Discrepancies in the Measured Data

The noise measurements were carried out in two sets of frequency range, one from 2 GHz to 26 GHz and the other from 26 GHz to 40 GHz. The probable reason for measuring the noise in the two frequency sets could be the bandwidth limitation of the noise source to generate a noisy signal. Hence, two different noise sources could have been used in the noise measurements over the stated frequency range. Because of the two different noise sources or entire different measurement set-up, the values

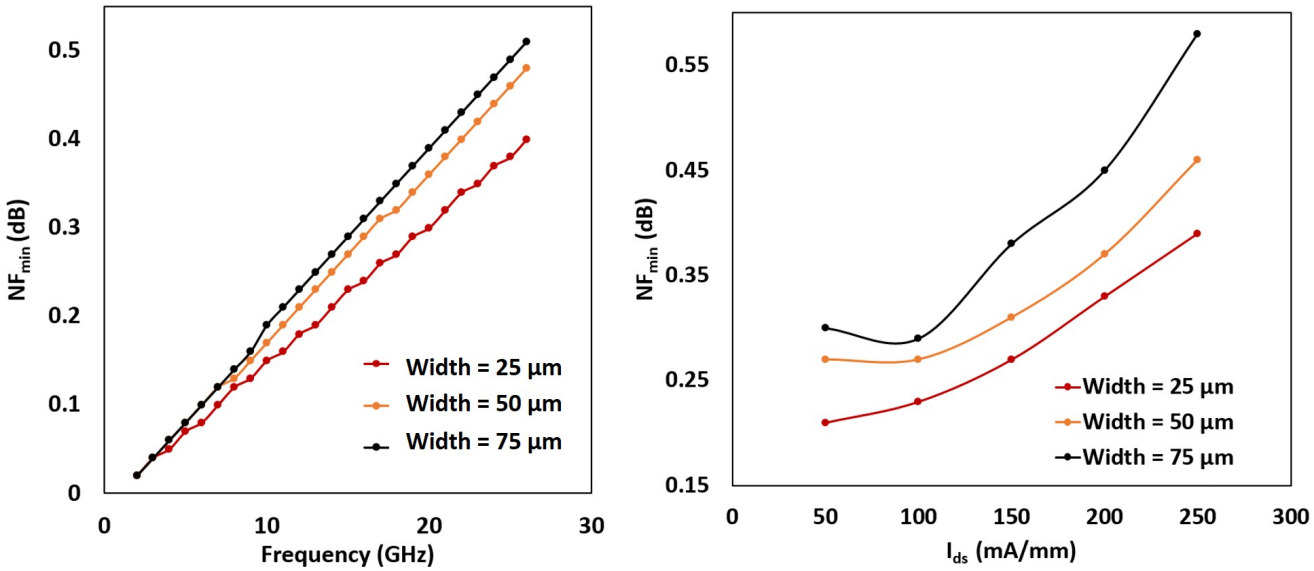

Figure 3.3: Response of measured NF_{min} (a) across the frequencies, when the three tested devices are biased to conduct a drain current (I_{ds}) of 100 mA/mm (b) across drain current I_{ds} at frequency 15 GHz, for three different device widths with number of gate fingers $= 8$

of the noise parameters are not only discontinuous at 26 GHz, but also the two set-ups recorded different noise behaviour for the same HEMT under the same test condition. Considering the lower reliability of a high-frequency noise source, the high-frequency measurement set-up is considered to be less accurate. This variability in the measurements is observed in the frequency response of all the three noise parameters as shown in Figure 3.4.

The minimum noise figure abruptly increases in the range of 0.21 dB to 0.26 dB at the juncture of the two measured frequency sets (26 GHz) across all device geometries and bias points, although its slope is similar in both measured sets as shown in Figure 3.4(a). It should be noted that the maximum observed minimum noise figure is not greater than 0.9 dB at 26 GHz across any device geometry or bias point. Therefore, the change in the measurement set-up has introduced an error of approximately 24% in the minimum noise figure. Similarly, both the optimum signal source admittance and the equivalent noise resistance abruptly increase at the common frequency point of the two measured data sets, although the rise is not as high as for the minimum noise figure. Thereafter, their values continue to decrease as shown in Figures 3.4(b) and 3.4(c). Furthermore, peculiar values in the optimum signal source admittance's frequency response are noted at the initial low frequencies as shown in Figure 3.4(b). Such a response has not been observed in the past literature, hence it is difficult to evaluate its genuineness.

The deviation in values of the analytical minimum noise figure at higher frequencies and in values of the optimum signal source admittance at the initial frequencies from their corresponding measured data are to be expected. With an understanding of the potential inaccuracies in the measurement

data, a more meaningful comparison can be done between the analytical noise parameters and the measured data to obtain the unknowns in the expressions of the noise currents.

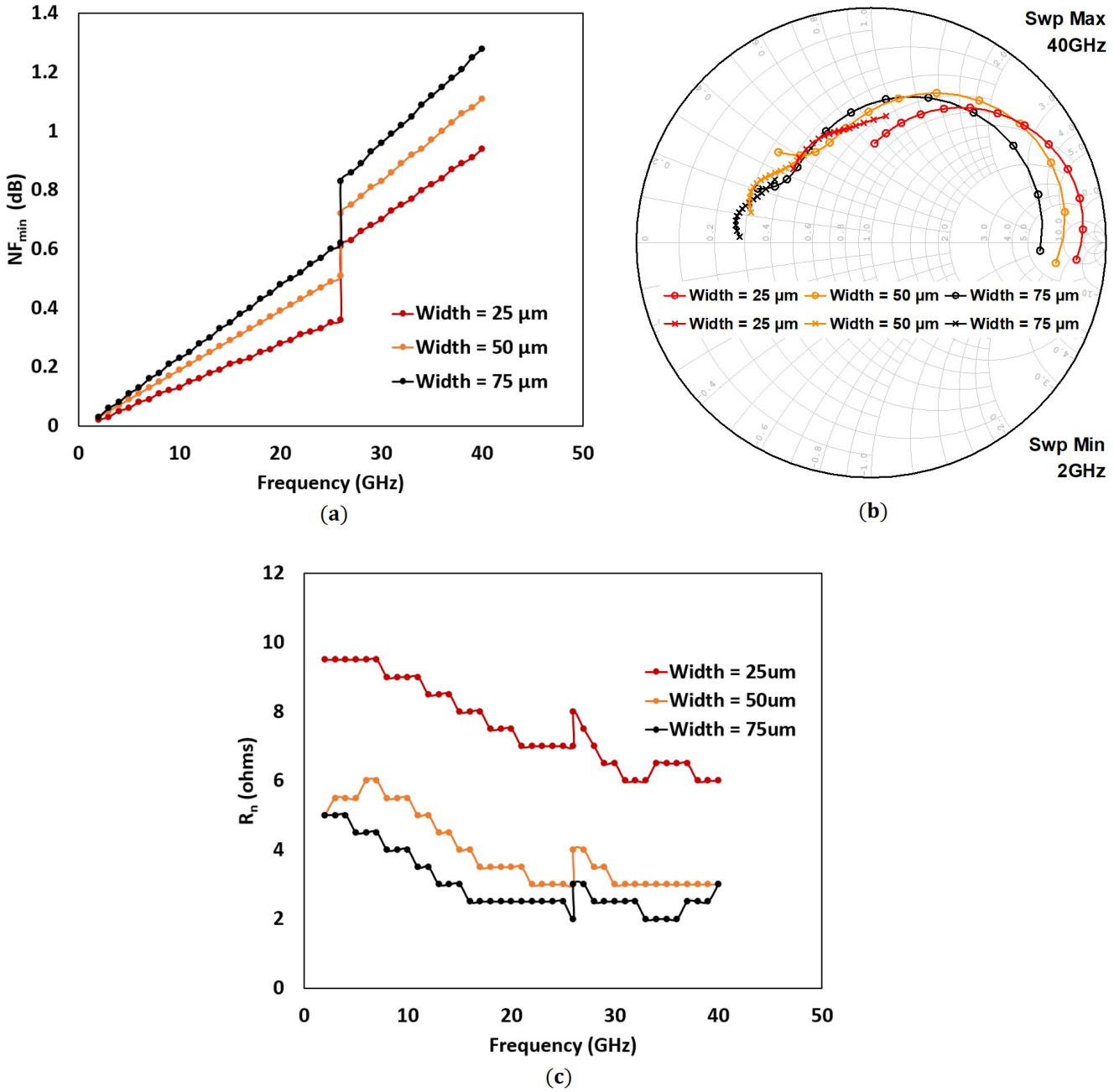

Figure 3.4: Response of measured noise parameters: (a) Minimum noise figure (NF_{min}) (b) Normalised optimum signal source admittance (Y_{opt}) (c) Equivalent noise resistance (R_n) with frequency for various device geometries biased to conduct a drain current (I_{ds}) of 100 mA/mm. The jump at 26 GHz is due to the use of two different measurement set-ups

3.6 Results and Discussion

The analytical noise parameters can be obtained by inserting the expression for the spectral density of the drain and gate noise currents (equations (3.21) and (3.30)) in the expression for the spectral

density of the input noise voltage and current (equations (2.3) and (2.4)). In the normal bias conditions, it can be assumed that the fluctuating channel charge is distributed equally ($50\% - 50\%$) between the source and the drain regions under the gate, hence γ_{sd} is set at 0.5 in the noise model. On comparing the analytical noise parameters with the measured parameters, it is observed that small fractional values of both the constants (N_{ds} and $\overline{q_{cc}}$) can produce a close fit between the noise parameters as shown in Figure 3.5 and Figure 3.8, along with a few exceptions. These exceptions with their underlying reasons and remedies are discussed below:

- The measured optimum signal source admittance for any given device geometry decreases with an increase in frequency as shown in Figure 3.5, whereas the measured noise figure of the HEMT increases with frequency as observed in Figure 3.6. Although, both the analytically obtained noise parameters follow the same trend, at higher frequencies the change in the slope of their response is not as sharp as in the case of the measured data. Such a response of the analytical parameters was anticipated, both the reason and the analysis of which are discussed below:
  - Since the spectral density of the drain-noise current is independent of frequency while the frequency-dependent gate-noise current is small in magnitude compared to the drain-noise current, the noise figure cannot be expected to increase at an approximately linear rate.
  - Furthermore, the response of an equivalent noise resistance which is mainly dependent on the gate-noise current, except for low frequencies, is closely aligned with the measured data as shown in Figure 3.7. This confirms that there is no need for further amendments in the analysis of the gate-noise current to predict the high-frequency noise performance of the HEMT.
  - Thus, an additional frequency-dependent drain-noise current is needed to correctly model the noise performance of the HEMT at high frequencies. Both the physical origin and its expression are discussed in the next chapter.
- The analytically obtained minimum noise figure is significantly lower than for the measured data over the frequency range as shown in Figure 3.8. The reason for the lower analytical minimum noise figure is discussed below:
  - In the equations (3.21) and (3.30) both the drain and gate noise currents are considered to be completely correlated to each other since they share exactly the same randomness in their distribution, having originated from the same source.
  - However, according to noise theory, the drain-noise current must be composed of two components, one completely correlated to gate-noise current, the other completely uncorrelated to it. Because the latter component is missing in the expression of the minimum noise figure (equation (2.12)), the analytical parameter falls below the measured parameter.

– This reason is further validated from the response of the noise figure of the device as shown in Figure 3.6. The analytically obtained noise figure is closely related to the measured data in the low-frequency spectrum and deviates at high frequencies because of the absence of the frequency-dependent drain-noise current source and due to the additional noise in the high-frequency set-up.

– Hence, the right correlation between the drain-noise current and the gate-noise current, by sub-dividing the drain-noise current into two components, can match the analytical minimum noise figure with the measured data. Further details on the expression of their correlation coefficient will be discussed in the next chapter.

Thus, the comparisons of the analytical noise parameters with their corresponding measured results indicates that the gate and the drain-noise currents are not completely correlated to each other but only partially. Furthermore, random fluctuations in the number of charge carriers in the channel per unit time are not sufficient to explain the noise performance of the HEMT at high frequencies. An additional noise source is needed to completely predict the HEMT's noise performance.

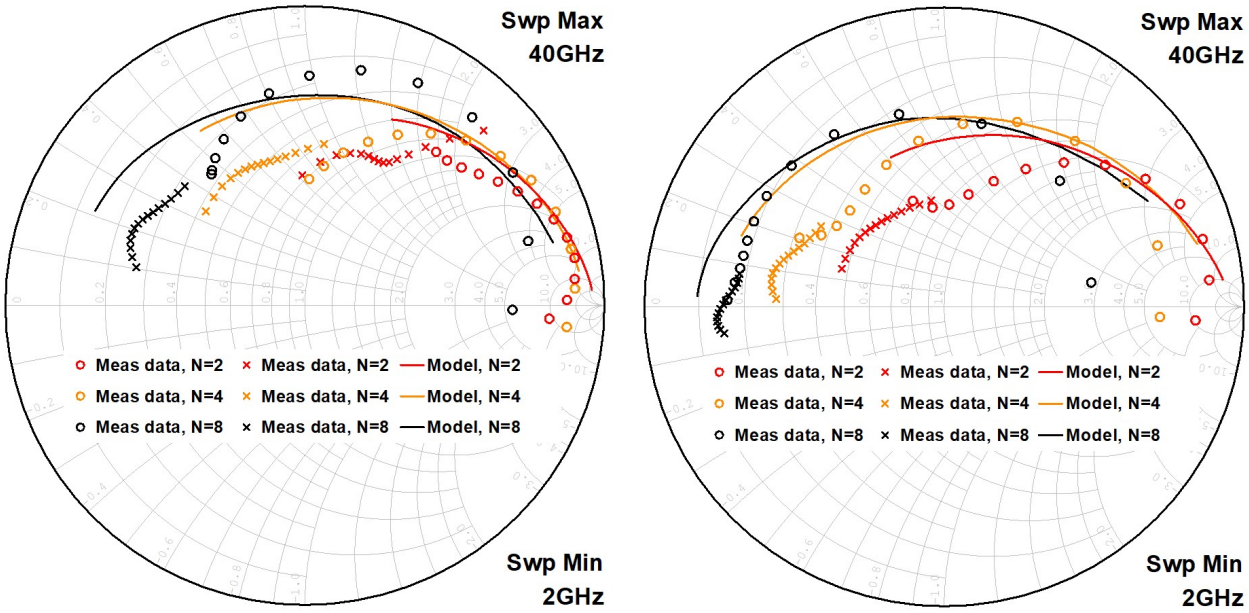

Figure 3.5: A comparison between the measured (in circles and crosses) and analytically obtained (in solid lines) normalised optimum signal source admittances ($\frac{Y_{opt}}{Y_0}$) over the two extreme device widths: (a) device width equal to 25 μm and (b) device width equal to 75 μm, for all gate fingers biased to conduct a drain current (I_{ds}) of 100 mA/mm across the entire discussed frequency spectrum. Circles represent low frequency measured data sets and crosses represent high frequency measured data sets

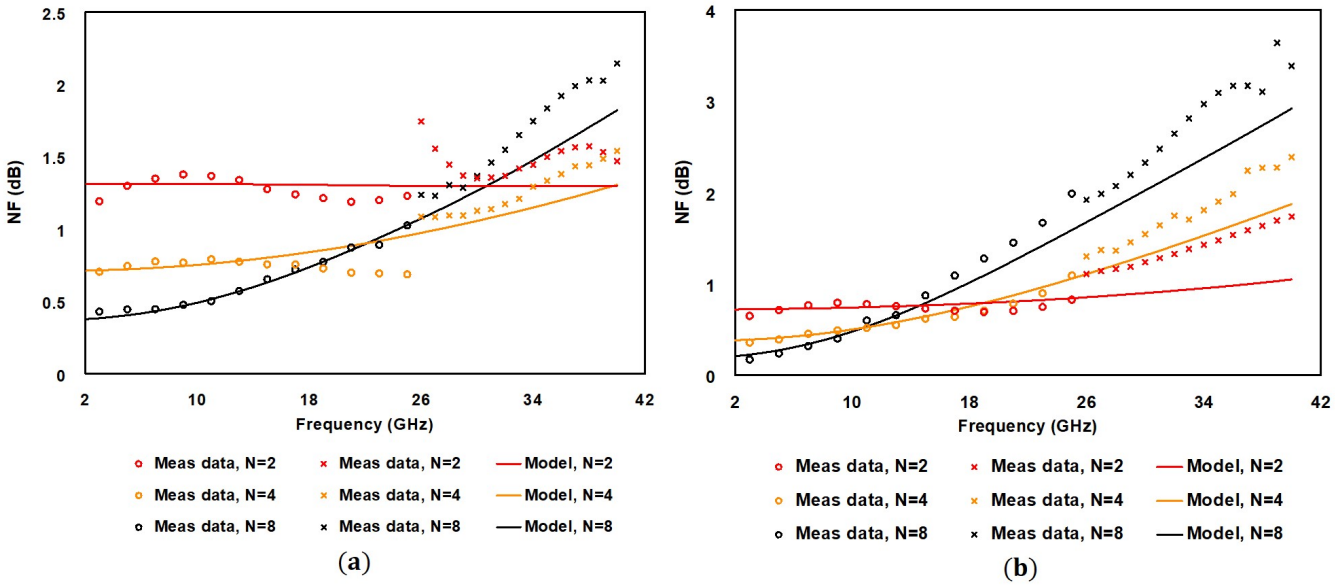

Figure 3.6: A comparison between the measured (in circles and crosses) and analytically obtained (in solid lines) noise figures (NF) over the two extreme device widths: (a) device width equal to 25 μm and (b) device width equal to 75 μm, for all gate fingers biased to conduct a drain current (I_{ds}) of 100 mA/mm across the entire discussed frequency spectrum. Circles represent low frequency measured data sets and crosses represent high frequency measured data sets

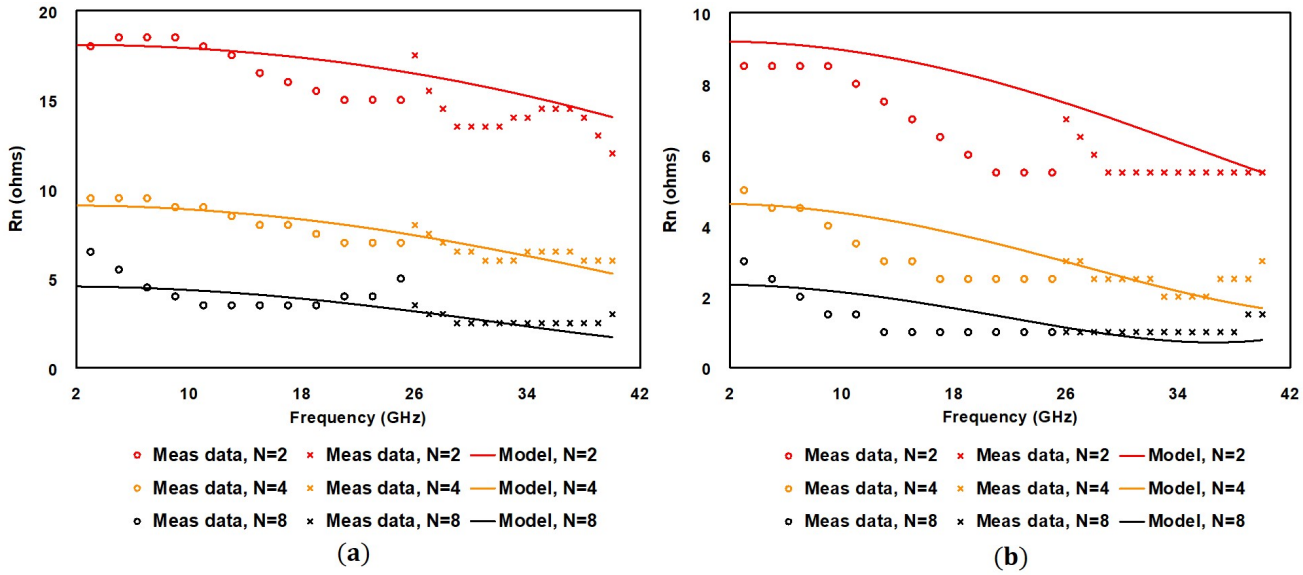

Figure 3.7: A comparison between the measured (in circles and crosses) and analytically obtained (in solid lines) equivalent noise resistances (R_n) over the two extreme device widths: (a) device width equal to 25 μm and (b) device width equal to 75 μm, for all gate fingers biased to conduct a drain current (I_{ds}) of 100 mA/mm across the entire discussed frequency spectrum. Circles represent low frequency measured data sets and crosses represent high frequency measured data sets

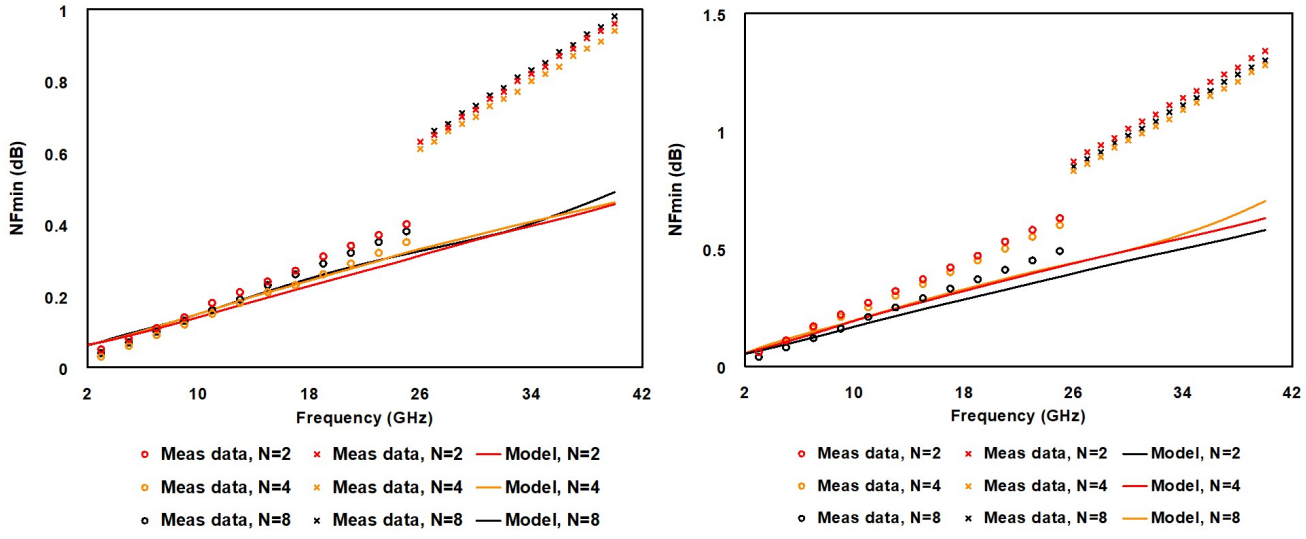

Figure 3.8: A comparison between the measured (in circles and crosses) and analytically obtained (in solid lines) minimum noise figures (NF_{min}) over the two extreme device widths: (a) device width equal to 25 μm and (b) device width equal to 75 μm, for all gate fingers biased to conduct a drain current (I_{ds}) of 100 mA/mm across the entire discussed frequency spectrum. Circles represent low frequency measured data sets and crosses represent high frequency measured data sets

3.7 Conclusion

The origin of the drain-noise current appears to be "non-thermal" in sub-micrometre HEMT devices. On the other hand, the noise phenomenon in the HEMT is found to be due to the random fluctuations in the large number of charge carriers traversing the channel per unit time. Therefore, the analytical expression for the spectral density of the correlated noise currents is determined using probability theory by considering that these random fluctuations constitute a Poisson distribution. With the help of these analytical expressions, a noise model for the HEMT which is scalable across different device geometries is developed.

Due to the use of different noise measurement set-ups across the two frequency sets, approximately 24% error is observed in the measurements of the minimum noise figure at the juncture of the two measured data sets. Similar inaccuracies are also observed in the frequency response of the other measured noise parameters. Apart from these measurement errors, the noise model is able to predict the noise performance of HEMT in close alignment with the accurate measured data.

It is also observed that the two noise currents are not completely correlated to each other, as hypothesised by the two-port noise theory. Hence, an additional drain-noise current source is required which is completely uncorrelated to the gate current to accurately determine the minimum noise figure of the HEMT. Furthermore, the noise performance of the HEMT at the higher frequencies cannot be explained by considering only the gate-noise current to be frequency dependent. Hence,

another frequency-dependent drain-noise current source is needed to explain the high-frequency noise performance of the HEMT. The physical origin and expression for spectral density of both the additional noise-current sources along with the final results of the model are discussed in the next chapter.

Chapter 4

Complete Non-linear Noise Model

This chapter describes both the physical origin and a mathematical expression for the frequency-dependent drain-noise current. Thereafter, the channel-noise current is revised to include a noise component uncorrelated with the gate-noise current. With the use of these three noise-current sources, a scalable non-linear noise model written in Verilog-A is described in this chapter. Furthermore, to validate the effectiveness of the model, the response of the analytical noise parameters are compared with the corresponding measured parameters. Also, to describe the need for and utility of the model, a comparison between the noise parameters calculated from the described model and the noise model provided by WIN Semiconductor Corporation is carried out. In the end, to verify the functionality of the model, the noise model is integrated into the existing non-linear model and a comparison between the S-parameters calculated using the integrated model and obtained from measurements is shown.

4.1 Frequency-Dependent Drain-Noise Current

The leakage current between the source and drain terminals of the HEMT through the buffer layer or doped layer has been reported many times in the literature [42]. Therefore, many successful efforts have been carried out to minimise the leakage [43, 44]. However, the number of charge carriers and the associated random fluctuations in the buffer layer or in the doped layer are still significant enough to generate a noise current. The random fluctuations in the number of charge carriers arriving at the drain terminal through the buffer layer or doped layer are for two reasons: first is the dislocation of the atoms at the interface and second is the uncertainty in predicting accurately their momentum and position simultaneously at the same time. The atom dislocations at the interface cause either carrier scattering or trapping. Since the mechanisms resulting in these random fluctuations are only partially different from the one in the channel, the two noise sources can be considered as partially correlated with each other.

4.1.1 Mathematical Description of Frequency-Dependent Drain Current

Let N_{bl} be the number of charge carriers inside the buffer layer or doped layer at a time instant τ between the drain and source terminals, hence the charge inside the buffer layer or in the doped layer will be $q_{bl}\,(=q\,N_{bl})$. The charge spectral density [C^2/Hz] of the overall random fluctuations in the charge (q_{nbl}) for the discussed reasons can be given as

$$\frac{\overline{q_{nbl}^2}}{\Delta f} = \frac{\overline{q_{nblc}^2}}{\Delta f} + \frac{\overline{q_{nblu}^2}}{\Delta f} \tag{4.1}$$

where $\overline{q_{nblc}^2}$ represents the variance in the charge due to the uncertainty in predicting momentum and position simultaneously and $\overline{q_{nblu}^2}$ represents the variance in the charge due to the dislocations of atoms at the interface.

From equation (3.24)

$$\frac{\overline{q_{nblc}^2}}{\Delta f} = 2\,q\,\overline{q_{blc}} \tag{4.2}$$

$$\frac{\overline{q_{nblu}^2}}{\Delta f} = 2\,q\,\overline{q_{blu}} \tag{4.3}$$

where $\overline{q_{blc}}$ and $\overline{q_{blu}}$ represent the charge associated with the average number of charge carriers (N_{blc} and N_{blu}) present in the buffer layer or the doped layer at time τ. The units of $\overline{q_{blc}}$ and $\overline{q_{blu}}$ are [C/Hz].

Hence, the total noise charge present inside the buffer layer or in the doped layer, with the condition that both noise sources are independent of each other, will be given as

$$q_{nbl} = \sqrt{2\,q\,\overline{q_{blc}}\,\Delta f} + \sqrt{2\,q\,\overline{q_{blu}}\,\Delta f} \tag{4.4}$$

The noise current [A] flowing between the drain and source terminals due to the random fluctuations in the charge (q_{nbl}) present in the buffer layer or in the doped layer can be given as

$$i_{nbl}(\omega) = j\,\omega\,q_{nbl} \tag{4.5}$$

$$i_{nbl}(\omega) = j\,\omega\,\left(\sqrt{2\,q\,\overline{q_{blc}}\,\Delta f} + \sqrt{2\,q\,\overline{q_{blu}}\,\Delta f}\right) \tag{4.6}$$

Thus, the noise current is a function of frequency. The spectral density of the noise current [A^2/Hz] due to random fluctuations in the buffer layer or in the doped layer charge is given as

$$\frac{\overline{i_{nbl}^2}}{\Delta f} = 2\,\omega^2\,q\,(\overline{q_{blc}} + \overline{q_{blu}}) \tag{4.7}$$

4.1.2 Verilog-A Implementation of Frequency-Dependent Drain Current

As the channel-noise current and frequency-dependent drain-noise current are partially correlated with each other, the variance in the noisy charge inside the buffer layer or in the doped layer must be represented by two different "white_noise()" functions with the same variance of 2q such as

$$\sigma_{blc} = white\_noise(2q)\,; \tag{4.8}$$

$$\sigma_{blu} = white\_noise(2q)\,; \tag{4.9}$$

Hence, the noisy charge in the buffer layer or in the doped layer $[\mathrm{C}/\sqrt{\mathrm{Hz}}]$ can be described in Verilog-A using equation (4.4) as

$$q_{nbl} = \sigma_{blc}\sqrt{\overline{q_{blc}}} + \sigma_{blu}\sqrt{\overline{q_{blu}}}\,; \tag{4.10}$$

Finally, the terminal drain-noise current $[\mathrm{A}/\sqrt{\mathrm{Hz}}]$ due to the noisy charge in the buffer layer or the doped layer can be obtained by taking the time derivative of equation (4.10) as

$$I(d,s) <+ \sqrt{\overline{q_{blc}}}\,ddt\{\sigma_{blc}\} + \sqrt{\overline{q_{blu}}}\,ddt\{\sigma_{blu}\}; \tag{4.11}$$

4.1.3 Influence of Frequency-Dependent Drain Current on Noise Parameters

The high-frequency response of the noise parameters of the HEMT improves significantly with the addition of a partially correlated frequency-dependent drain-noise current as shown in Figure 4.1(b) - 4.2(b). The frequency-dependent drain-noise component is added only in part (b). The close match of the noise parameters with the high-frequency measured data in part (b) of both figures indicates the necessity of the frequency-dependent drain-noise current. However, the analytically obtained minimum noise figure is still lower than the corresponding measured data. Therefore, the channel-noise current must be revised again and an uncorrelated noise component must be added to the channel-noise current.

These figures indicate that, even though the contribution of the charge carriers inside the buffer layer or in the doped layer is almost negligible compared to the drain current, they cannot be neglected while describing the drain-noise current. This is because the order of the drain current is in mA but the noise current is in the order of $\mathrm{nA}/\sqrt{\mathrm{Hz}}$, hence fluctuations in small carrier densities in the buffer layer or in the doped layer can generate the small drain-noise current.

4.2 Revision of Channel-Noise Current

As shown in Figures 3.8 and 4.2, the measured minimum noise figure is larger than the corresponding analytical minimum noise figure, which is calculated with the assumption that both noise currents

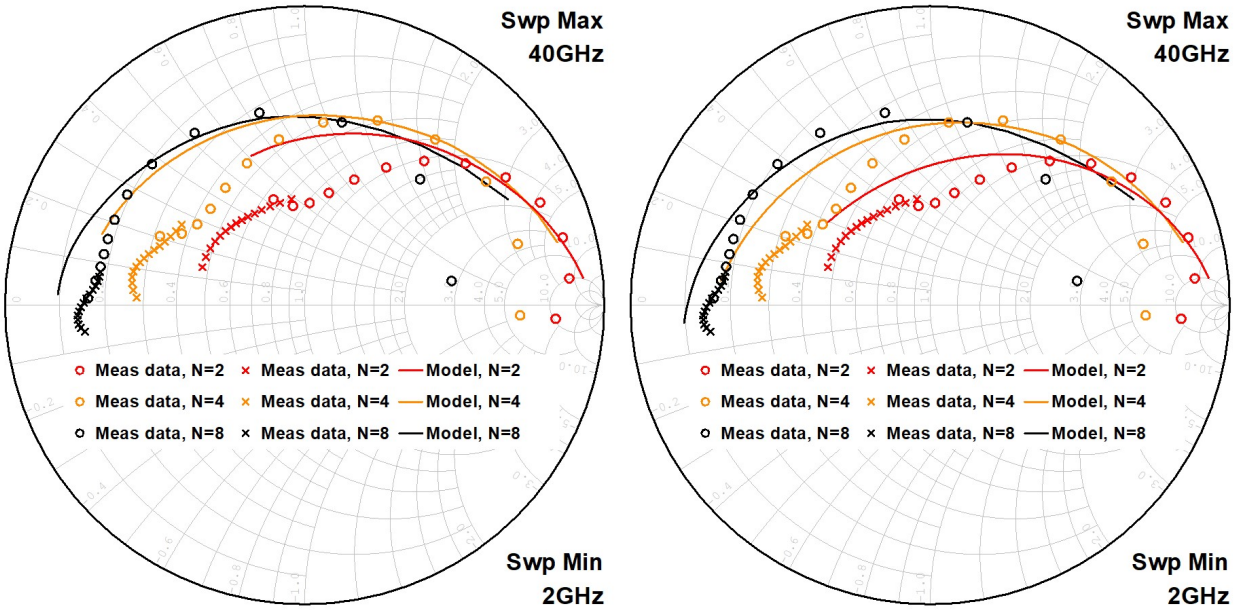

Figure 4.1: A comparison between the measured (in circles and crosses) and analytically obtained (in solid lines) normalised optimum signal source admittances: (a) Without frequency-dependent drain-noise current (b) With frequency-dependent drain-noise current, for a 75 μm wide device across all gate fingers biased to conduct a drain current (I_{ds}) of 100 mA/mm across the entire discussed frequency spectrum

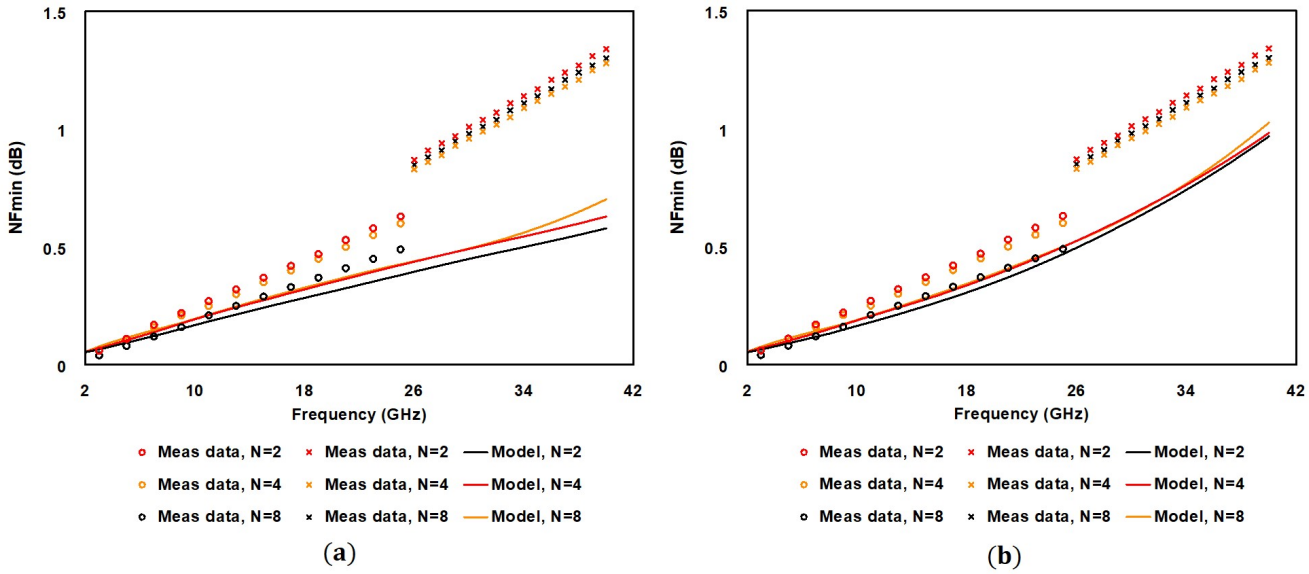

Figure 4.2: A comparison between the measured (in circles and crosses) and analytically obtained (in solid lines) minimum noise figures: (a) Without frequency-dependent drain-noise current (b) With frequency-dependent drain-noise current, for a 75 μm wide device across all gate fingers biased to conduct a drain current (I_{ds}) of 100 mA/mm across the entire discussed frequency spectrum

are completely correlated. However, as discussed in the noise theory of two-ports in Section 2.1, the two noise currents (drain and gate noise) are partially correlated with each other. Thus, with the guidelines of two-port noise theory, the channel-noise current [A] must be divided into two parts:

$$i_{nch} = i_{nchc} + i_{nchu} \tag{4.12}$$

where i_{nchc} and i_{nchu} are completely correlated and uncorrelated to the gate-noise currents and can be defined using equation (3.22)

$$i_{nchc} = \sqrt{2\, N_{dsc}\, q\, I_{ds}\, \Delta f} \tag{4.13}$$

$$i_{nchu} = \sqrt{2\, N_{dsu}\, q\, I_{ds}\, \Delta f} \tag{4.14}$$

where N_{dsc} and N_{dsu} are the corresponding scalar factors.

4.2.1 Verilog-A Implementation of Channel-Noise Current

Since both components of the channel-noise current are independent of each other even though both have the same variance of 2q, two different "white_noise()" functions must be needed, such as

$$\sigma_{chc} = white\_noise(2q)\,; \tag{4.15}$$

$$\sigma_{chu} = white\_noise(2q)\,; \tag{4.16}$$

Hence, the channel-noise current [$\mathrm{A}/\sqrt{\mathrm{Hz}}$] in Verilog-A is represented as

$$i_{nch} = \sigma_{chc}\, \sqrt{N_{dsc}\, I_{ds}} + \sigma_{chu}\, \sqrt{N_{dsu}\, I_{ds}}\,; \tag{4.17}$$

4.3 Revision of Noise Currents in the Model

The drain-noise current is the sum of the noise current in the buffer layer or in the doped layer (equation (4.6)) and the channel-noise current (equations (4.13)-(4.14)) is described as

$$i_{nd} = i_{nchc} + i_{nchu} + i_{nbl} \tag{4.18}$$

$$i_{nd} = \sqrt{2\, N_{dsc}\, q\, I_{ds}\, \Delta f} + \sqrt{2\, N_{dsu}\, q\, I_{ds}\, \Delta f} + j\,\omega \left(\sqrt{2\, q\, \overline{q_{blc}}\, \Delta f} + \sqrt{2\, q\, \overline{q_{blu}}\, \Delta f} \right) \tag{4.19}$$

The noise channel charge, which is coupled to the gate terminal through the capacitances C_{gs} and C_{gd} as mentioned in equations (3.26)-(3.27) can be given as

$$q_{ngd} = \sqrt{2\, q\, \overline{q_{cc}}\, \gamma_{sd}\, \Delta f} \tag{4.20}$$

$$q_{ngs} = \sqrt{2\, q\, \overline{q_{cc}}\, (1 - \gamma_{sd})\, \Delta f} \tag{4.21}$$

Thus, the total gate-noise current [A] associated with the coupling of the overall random fluctuations in the channel charge using equation (3.29) must be given as

$$i_{ng} = j\,\omega\,\sqrt{2\,q\,\overline{q_{cc}}\,\Delta f} \tag{4.22}$$

Hence, the partial correlation coefficient between the gate-noise current and drain-noise current using equations (4.19) and (4.22) is given as

$$c = \frac{\overline{i_{ng}^{*}\,i_{nd}}}{\sqrt{|i_{ng}|^2 |i_{nd}|^2}} \tag{4.23}$$

where the cross-variance $\left(\overline{i_{ng}^{*}\,i_{nd}}\right)$ between the two noise currents is given as

$$\overline{i_{ng}^{*}\,i_{nd}} = -\,j\,\omega\,2\,q\,\Delta f\,\sqrt{N_{dsc}\,\overline{q_{cc}}\,I_{ds}} + \omega^2\,2\,q\,\Delta f\sqrt{\overline{q_{cc}}\;\overline{q_{blc}}} \tag{4.24}$$

Thus, the covariance between the two noise currents is no longer purely imaginary but has a real component as well. And the square of the magnitude of drain and gate noise currents can be given as

$$|i_{nd}|^2 = 2\,q\,\Delta f\,\left[(N_{dsc} + N_{dsu})\,I_{ds} + \omega^2\,(\overline{q_{blc}} + \overline{q_{blu}})\right] \tag{4.25}$$

$$|i_{ng}|^2 = 2\,\omega^2\,q\,\overline{q_{cc}}\,\Delta f \tag{4.26}$$

The drain-noise current and the coupled gate charge can be added into the terminal currents [$\mathrm{A}/\sqrt{\mathrm{Hz}}$] in Verilog-A using equations (4.19) and (3.26)-(3.27) as

$$I(d,s) <+ (\sigma_{chc}\,\sqrt{N_{dsc}} + \sigma_{chu}\,\sqrt{N_{dsu}})\sqrt{I_{ds}} + \sqrt{\overline{q_{blc}}}\,ddt\{\sigma_{blc}\} + \sqrt{\overline{q_{blu}}}\,ddt\{\sigma_{blu}\} \tag{4.27}$$

$$I(g,d) <+ \sqrt{\overline{q_{cc}}\gamma_{sd}}\;ddt\{\sigma_{chc}\}\,; \tag{4.28}$$

$$I(g,s) <+ \sqrt{\overline{q_{cc}}(1-\gamma_{sd})}\;ddt\{\sigma_{chc}\}\,; \tag{4.29}$$

where $\sigma_{blc} = \sigma_{chc} + \sigma_{chu}$

Thus, the equations (4.27)-(4.29) describe the noise behaviour of the HEMT across various device geometries and bias points. The methodology of extracting the five unknowns (N_{dsc}, N_{dsu}, $\overline{q_{blc}}$, $\overline{q_{blu}}$ and $\overline{q_{cc}}$) in these equations from the response of the noise parameters with frequency is discussed in Section 4.4. Furthermore, the variation of the scalar factors N_{dsc} and N_{dsu} and the noise charges $\overline{q_{blc}}$, $\overline{q_{blu}}$ and $\overline{q_{cc}}$ with device geometries and bias points are described in Section 4.5.

4.4 Extraction Methodology of Model Parameters

There are five model parameters which are used in the expression of the three noise currents in equations (4.27)-(4.29). Two parameters are scalar quantities, N_{ds} and N_{dsu}, while three are average

charges per unit hertz $\overline{q_{cc}}$, $\overline{q_{blu}}$ and $\overline{q_{blc}}$. The values of these unknown parameters can be obtained by comparing the response of the analytical and measured noise parameters with frequency using curve fitting technique. These parameters scale with the device width and drain current.

The physical significance of each model parameter and the method of extracting these parameters are explained below:

- The first parameter that must be extracted is N_{ds}, which represents the fraction of the fluctuations in the channel charge carriers which reach the drain terminal with respect to the total fluctuations in the channel. Hence, its value is less than one. Parameter N_{ds} can be obtained from the variation of the equivalent noise resistance (R_n) with frequency. Since, at 2 GHz, the value of R_n primarily depends on the channel-noise current, the value of the model parameter N_{ds} is only tuned to match the analytical noise parameter R_n with the corresponding measured parameter at 2 GHz.

- The average of the total charge which gets coupled to the gate in time τ is represented by $\overline{q_{cc}}$ $[C/Hz]$. After freezing the value of N_{ds}, it can be extracted from the variation of the normalised optimum signal source admittance $\frac{Y_{opt}}{Y_0}$ with frequency. Therefore, its value is tuned until the analytical noise parameter $\frac{Y_{opt}}{Y_0}$ matches with the corresponding measured parameter at low frequencies.

- The average of the total charge that reaches the drain terminal through the buffer layer or the doped layer in time τ is represented by $\overline{q_{blu}}$ and $\overline{q_{blc}}$ with units $[C/Hz]$. After freezing the value of N_{ds} and $\overline{q_{cc}}$, the values of both noise charges are tuned simultaneously to match the analytical $\frac{Y_{opt}}{Y_0}$ with the measured parameter at high frequencies.

- The physical significance of both parameters N_{ds} and N_{dsu} are the same, with the only difference that N_{dsu} represents that fraction of the fluctuations in the number of channel charge carrier that are uncorrelated with the channel charge carriers which are coupled to the gate terminal. Its value is tuned to match the analytical NF_{min} with the corresponding measured parameter.

4.5 Scaling of Model Parameters

To develop a scalable noise model, each model parameter must scale with device geometry and drain current. The correlated noise factor N_{ds} was seen to decrease with the normalised drain current while the uncorrelated noise factor N_{dsu} increases with the normalised drain current but decreases with the

normalised device width. The scaling of both noise model parameters is given as

$$N_{ds} = F_{ds} \sqrt[4]{\frac{1e-3}{I_{ds}}} \tag{4.30}$$

$$N_{dsu} = F_{dsu} \sqrt[4]{\frac{I_{ds}}{1e-3}} \left(\frac{I_{ds}}{1e-3} \frac{25}{W} \right) \tag{4.31}$$

where W is the device width ranging from 25 μm to 75 μm. And $1e-3$ represents 1 mA.

Also, the average of the total coupled charge ($\overline{q_{cc}}$) with unit $[C/Hz]$ is seen to increase with both the normalised drain current and the normalised device width as

$$\overline{q_{cc}} = F_{cc}\ q \sqrt{\frac{I_{ds}}{1e-3} \frac{W}{25}} \tag{4.32}$$

The average of the total charge in the buffer layer or in the doped layer ($\overline{q_{blc}}$ and $\overline{q_{blu}}$) with units $[C/Hz]$ is seen to increase with the normalised drain current but decreases with the normalised device width as

$$\overline{q_{blc}} = F_{blc}\ q \left(\frac{25}{W} \right)^{\frac{3}{4}} \left(\frac{I_{ds}}{1e-3} \right) \tag{4.33}$$

$$\overline{q_{blu}} = F_{blu}\ q \sqrt{\frac{25}{W}} \left(\frac{I_{ds}}{1e-3} \right) \tag{4.34}$$

The values of the scalar factor used in the model are given in the following table

Scalar Factor	F_{ds}	F_{dsu}	F_{cc}	F_{blc}	F_{blu}
Value	0.34	0.0037	1.60	0.75	4.50

4.6 Results and Discussion

As defined in Section 4.5, all the five unknowns are the functions of drain current and device geometry. Furthermore, the noise currents are dependent on the dc drain current rather than on the changes in the drain current or on any linear device parameters like r_{gs} or g_{ds}, thus the noise model cannot be considered as a linear model. Hence, for a given value of the unknowns, a scalable non-linear noise model can be developed. The response of the analytical noise parameters, obtained using equations (4.27)-(4.29), fits very well with their corresponding measured data as shown in Figures 4.3 - 4.6. The response of four different device dimensions, biased at three different gate voltages to conduct 50 mA/mm, 100 mA/mm and 200 mA/mm are shown in the above mentioned figures.

The major challenge for any noise model is to match both the analytical normalised optimum signal source admittance and the minimum noise figure with the measured data at the same time. However, as shown in Figures 4.3 and 4.4 both parameters are matched very well.

A brief summary of the response of the analytical noise parameters is discussed below:

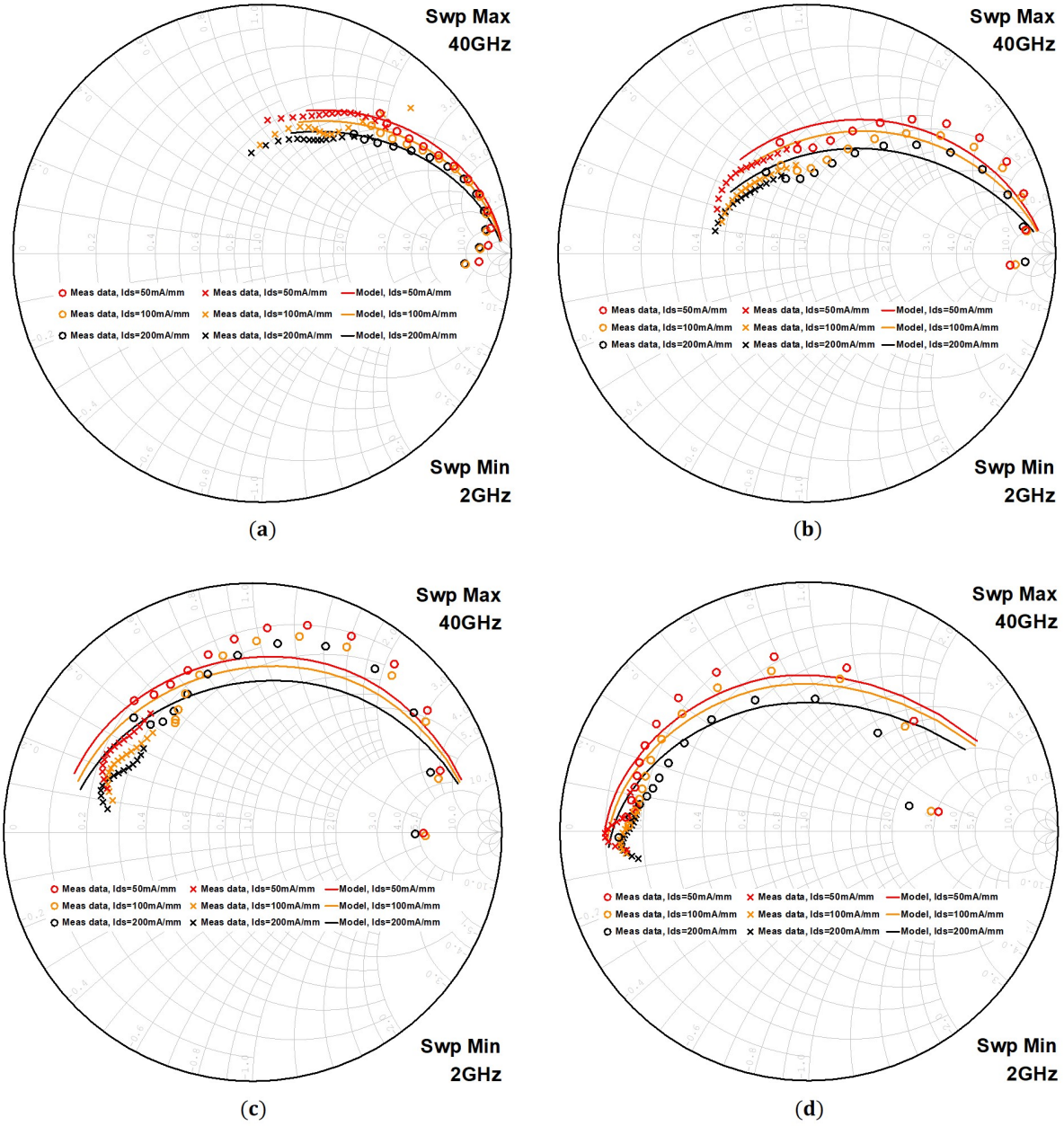

Figure 4.3: A comparison between the measured (in circles and crosses) and analytically obtained (in solid lines) normalised optimum signal source admittances over four device geometries: with device width equal to 25 μm (a) with two gate fingers and (b) with eight gate fingers; and with device width equal to 75 μm (c) with two gate fingers and (d) with eight gate fingers, biased to conduct three drain current (I_{ds}) values of 50 mA/mm, 100 mA/mm and 200 mA/mm across the entire discussed frequency spectrum

- The analytically obtained optimum signal source admittance is slightly larger than the measured data for an eight-finger gate device as shown in Figure 4.3(c) and 4.3(d) as compared to a two-finger gate device in Figure 4.3(a) and 4.3(b). One reason for the slightly higher value of the analytical optimum signal source admittance could be the uncorrelated sources associated with each finger. Every discussed noise source is defined for each individual gate finger rather than for the total fingers to ensure that all fingers have uncorrelated noise sources. Hence,

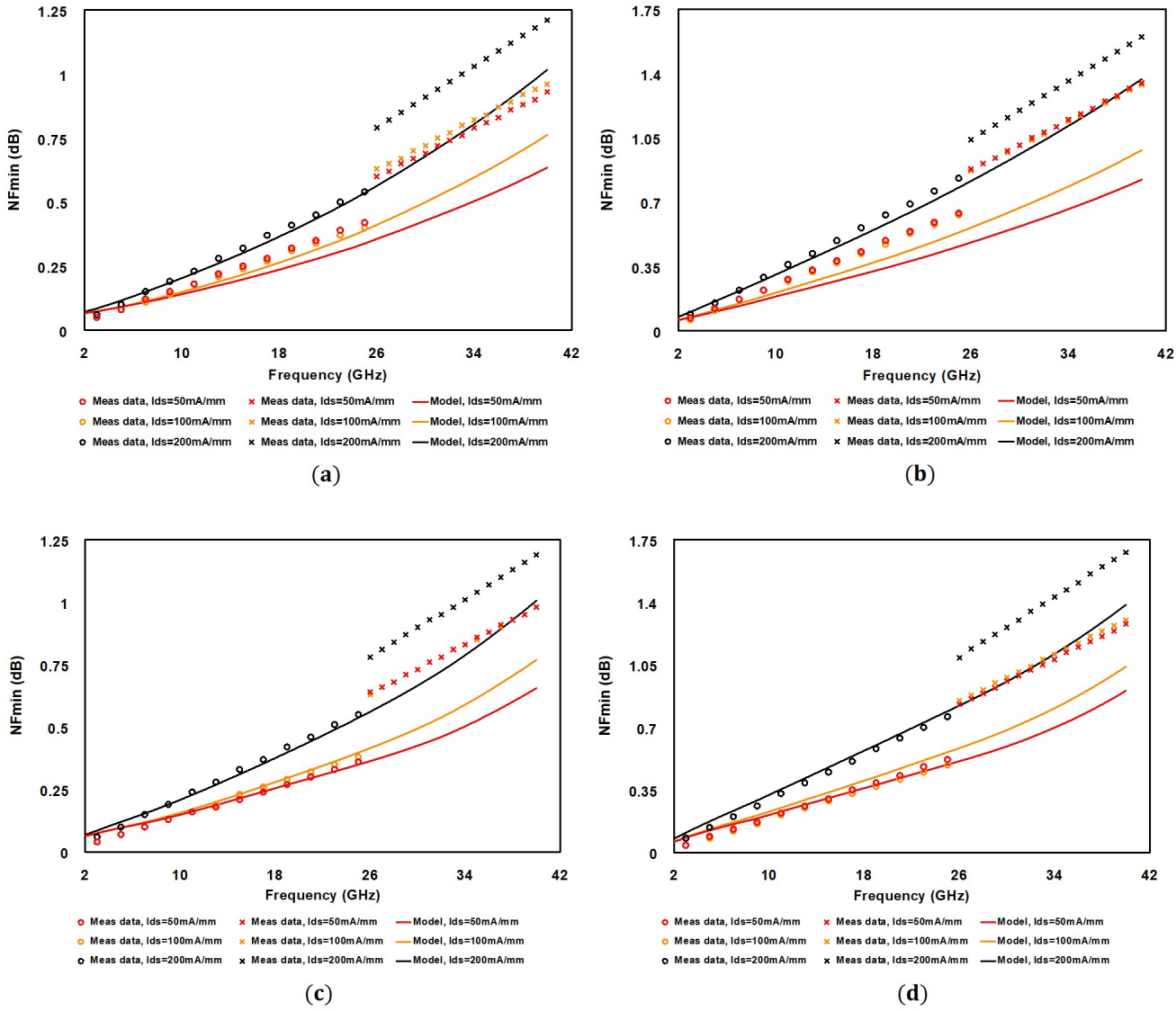

Figure 4.4: A comparison between the measured (in circles and crosses) and analytically obtained (in solid lines) minimum noise figures over four device geometries: with device width equal to 25 μm (a) with two gate fingers and (b) with eight gate fingers; and with device width equal to 75 μm (c) with two gate fingers and (d) with eight gate fingers, biased to conduct three drain current (I_{ds}) values of 50 mA/mm, 100 mA/mm and 200 mA/mm across the entire discussed frequency spectrum

this might cause a slight increase in the optimum signal source admittance for many fingered devices.

- With the inclusion of an uncorrelated channel-noise current, the minimum noise figure matches well with the measured results as shown in Figure 4.4. The measured minimum noise figure is similar for 50 mA/mm and 100 mA/mm drain currents, which could be because of the minimum resolution error in the measurements.

- The equivalent noise resistance is about $1\,\Omega - 2\,\Omega$ lower than its corresponding measured value

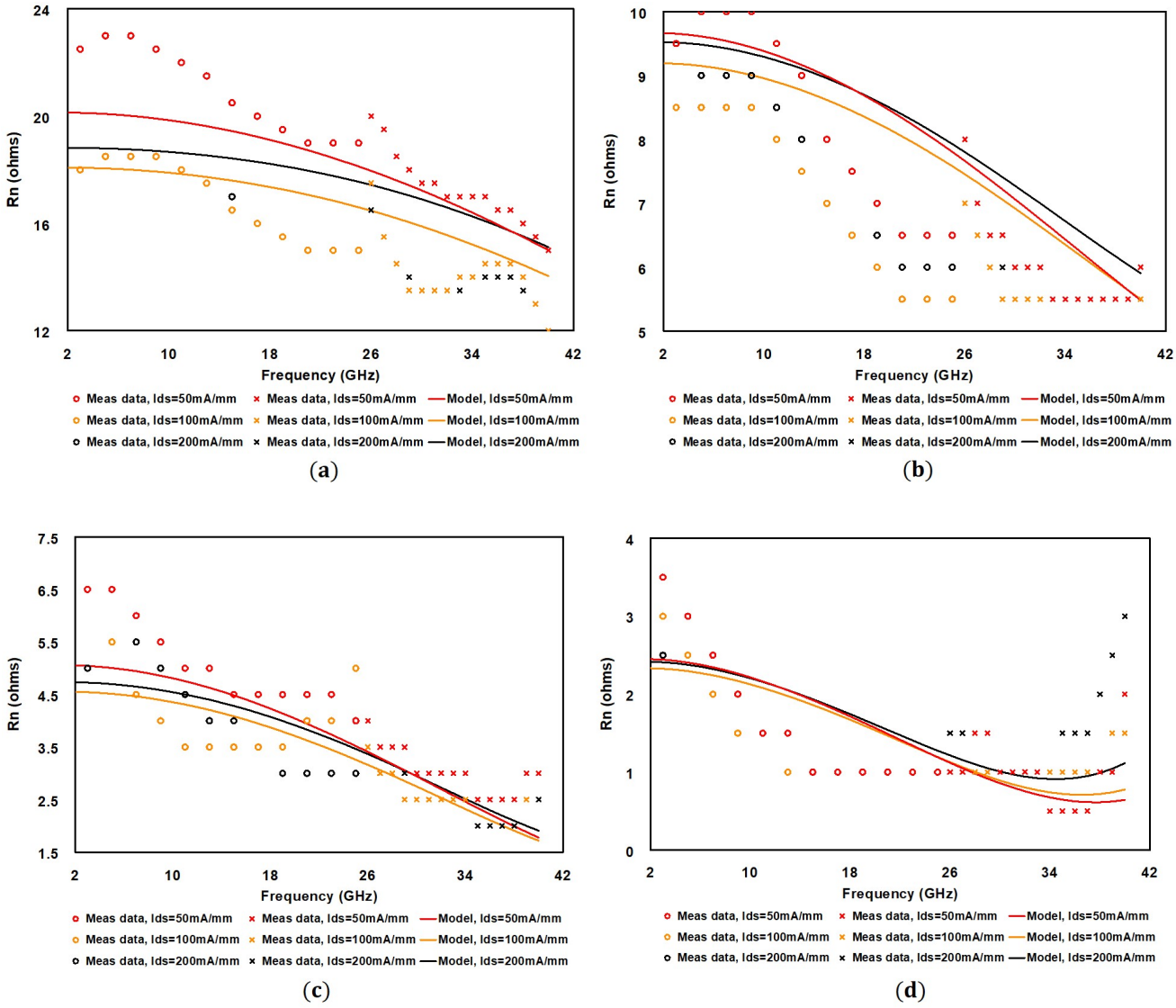

Figure 4.5: A comparison between the measured (in circles and crosses) and analytically obtained (in solid lines) equivalent noise resistances over four device geometries: with device width equal to 25 μm (a) with two gate fingers and (b) with eight gate fingers; and with device width equal to 75 μm (c) with two gate fingers and (d) with eight gate fingers, biased to conduct three drain current (I_{ds}) values of 50 mA/mm, 100 mA/mm and 200 mA/mm across the entire discussed frequency spectrum

for a drain current of 50 mA/mm in Figure 4.5 at the low frequencies. As pointed out above, the measured data for a 50 mA/mm drain current is considerably higher than the expected trend. Hence, this rise could be attributed to the error in measuring noise at such a low drain current.

- The bell-shaped response of the measured noise figure in Figure 4.6(a) and 4.6(b) at low frequencies does not appear to be a physical behaviour of the device, because this is only seen with a lower device width. Also, there is an offset of 0.25 dB and 0.28 dB between the two measured data sets in Figure 4.6(a) and 4.6(b).

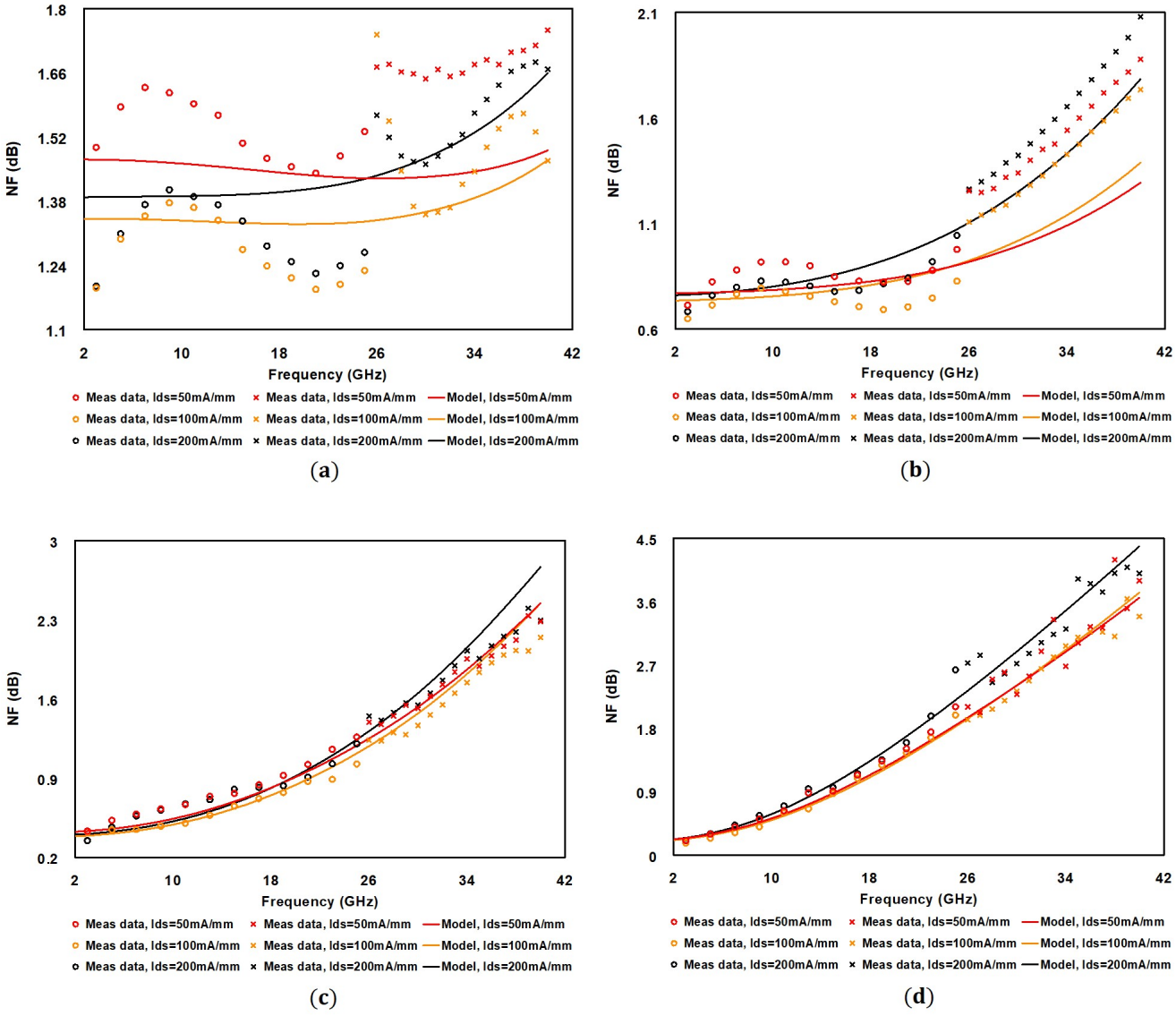

Figure 4.6: A comparison between the measured (in circles and crosses) and analytically obtained (in solid lines) noise figures over four device geometries: with device width equal to 25 μm (a) with two gate fingers and (b) with eight gate fingers; and with device width equal to 75 μm (c) with two gate fingers and (d) with eight gate fingers, biased to conduct three drain current (I_{ds}) values of 50 mA/mm, 100 mA/mm and 200 mA/mm across the entire discussed frequency spectrum

4.6.1 A Comparison with WIN Foundry Noise Model

In Figures 4.7 - 4.10, the noise parameters obtained from the two different models are compared with the measured data for the extreme device geometries at a single bias point. The other noise model used for comparison is from the WIN Semiconductor Corporation and is termed WIN's model. WIN's model is only able to match the minimum noise figure for low-frequency measured data out of the four noise parameters as shown in Figures 4.7 - 4.10. Since both models predict accurately the low frequency minimum noise figure, it confirms that extra noise gets added in the high-frequency measurement set-up or there might be some calibration error in high frequency measured data sets during the

measurement. Also, in Figure 4.7 the minimum noise figure calculated by WIN's model starts to decrease at higher frequency, which indicates that the model does not have a frequency-dependent drain-noise component, whereas our model predicts the required increase in the minimum noise figure at higher frequencies.

The magnitude of the normalised optimum signal source admittance corresponding to WIN's model is significantly higher than for the measured data as shown in Figure 4.8. This rise also contrasts with the fall in the minimum noise figure at higher frequencies obtained using WIN's model. On the other hand, the values of the equivalent noise resistance and the noise figure of the device obtained using WIN's model are lower than the measured results in Figures 4.9 and 4.10.

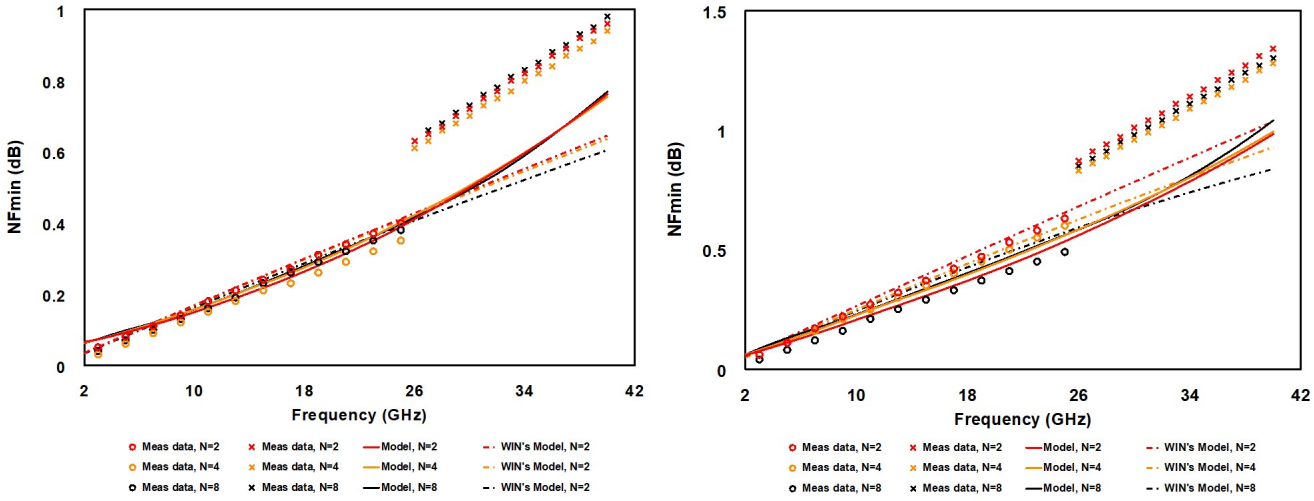

Figure 4.7: A comparison between the measured (in circles and crosses) and analytically obtained minimum noise figures from our model (in solid lines) and WIN's model (in broken lines) over the two extreme device widths: (a) device width equal to 25 μm and (b) device width equal to 75 μm, for all gate fingers biased to conduct a drain current (I_{ds}) of 100 mA/mm across the entire discussed frequency spectrum

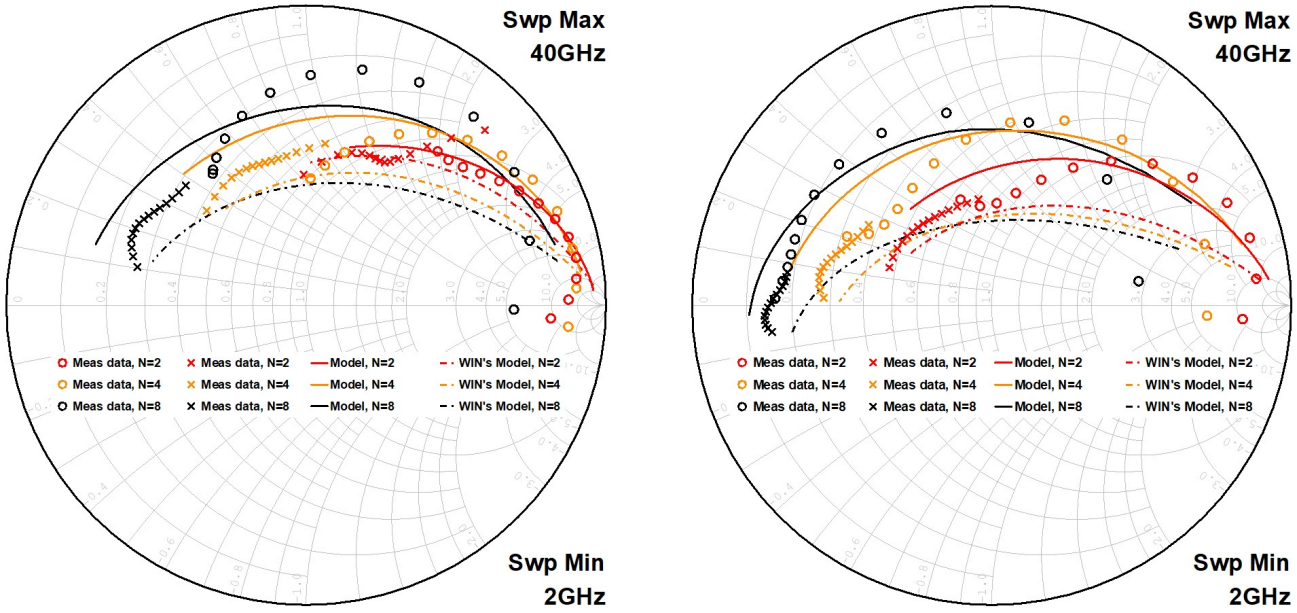

Figure 4.8: A comparison between the measured (in circles and crosses) and analytically obtained normalised optimum signal source admittances from our model (in solid lines) and WIN's model (in broken lines) over the two extreme device widths: (a) device width equal to 25 μm and (b) device width equal to 75 μm, for all gate fingers biased to conduct a drain current (I_{ds}) of 100 mA/mm across the entire discussed frequency spectrum

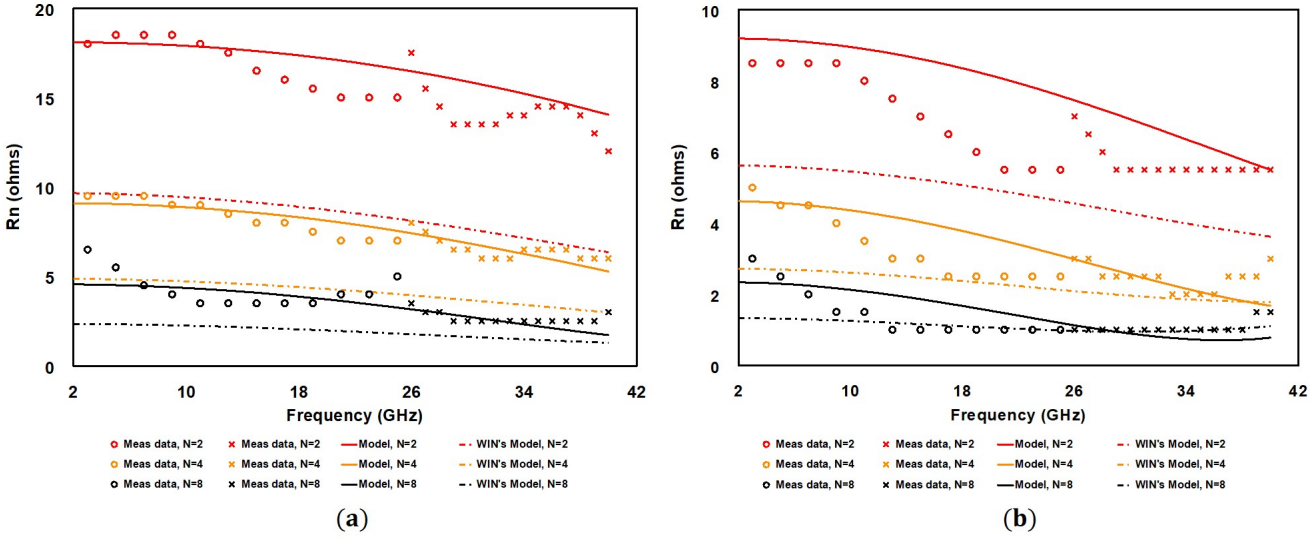

Figure 4.9: A comparison between the measured (in circles and crosses) and analytically obtained equivalent noise resistances from our model (in solid lines) and WIN's model (in broken lines) over the two extreme device widths: (a) device width equal to 25 μm and (b) device width equal to 75 μm, for all gate fingers biased to conduct a drain current (I_{ds}) of 100 mA/mm across the entire discussed frequency spectrum

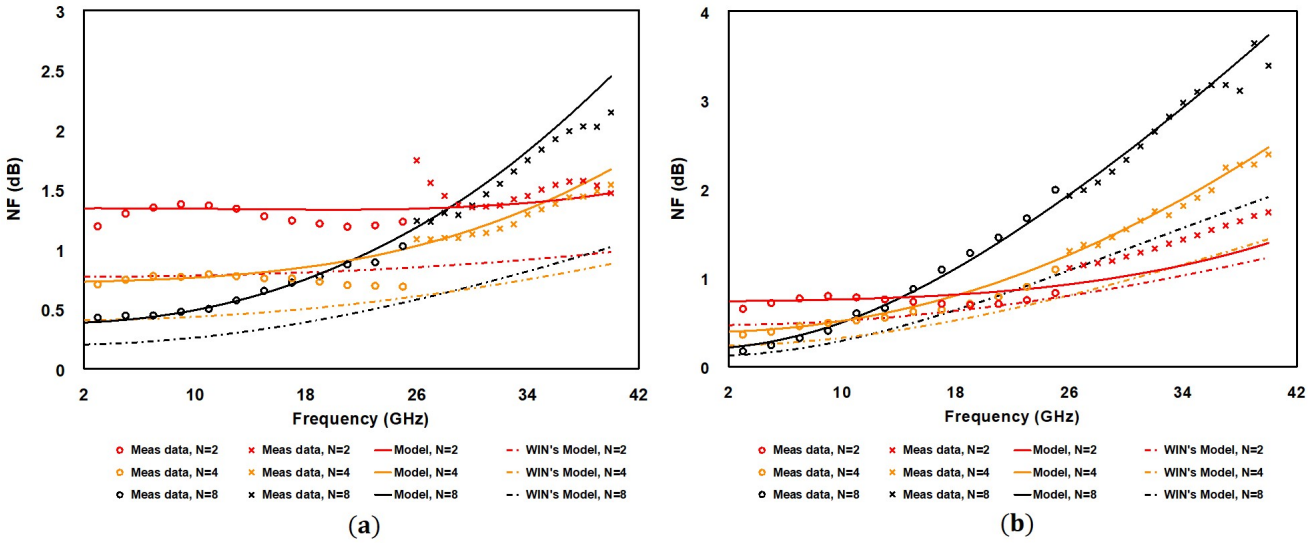

Figure 4.10: A comparison between the measured (in circles and crosses) and analytically obtained noise figures from our model (in solid lines) and WIN's model (in broken lines) over the two extreme device widths: (a) device width equal to 25 μm and (b) device width equal to 75 μm, for all gate fingers biased to conduct a drain current (I_{ds}) of 100 mA/mm across the entire discussed frequency spectrum

4.6.2 S-parameter Comparison

The proposed noise model is appended into the existing non-linear scalable model for an HEMT [45] to validate its functionality to be used as a non-linear model. As shown in Figures 4.11 - 4.14, the S-parameters of the device are closely aligned with the measured data, confirming that no additional parasitics are used in the model which can influence the normal operation of the device. Hence, the developed noise model can be easily appended into the existing non-linear model, and the integrated model can predict the noise and other device phenomena.

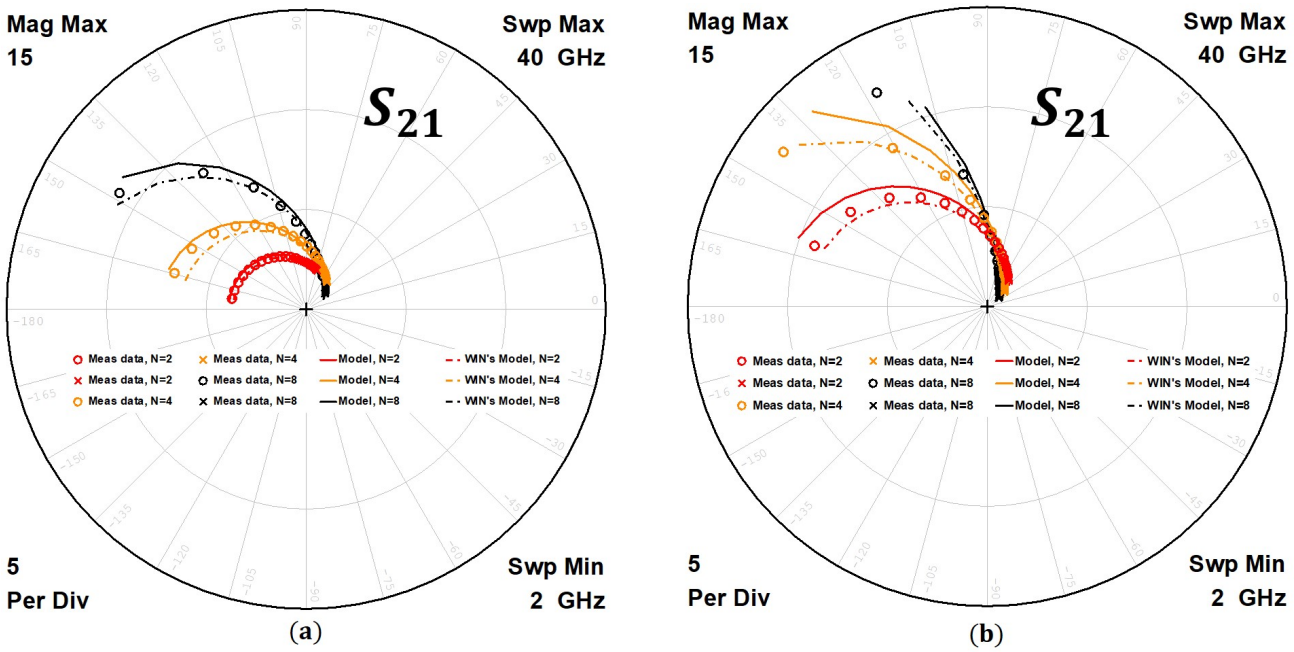

Figure 4.11: A comparison between the measured (in circles and crosses) and analytically obtained S_{21} from our model (in solid lines) and WIN's model (in broken lines) over the two extreme device widths: (a) device width equal to 25 μm and (b) device width equal to 75 μm, for all gate fingers biased to conduct a drain current (I_{ds}) of 100 mA/mm across the entire discussed frequency spectrum

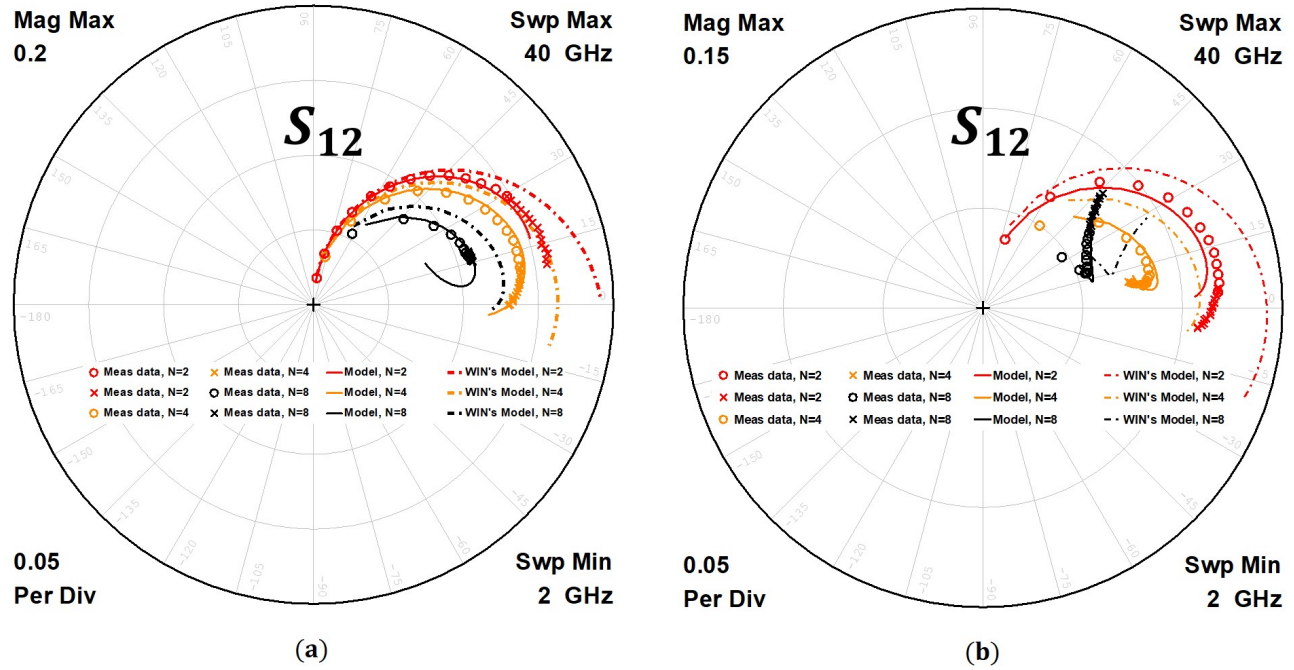

Figure 4.12: A comparison between the measured (in circles and crosses) and analytically obtained S_{12} from our model (in solid lines) and WIN's model (in broken lines) over the two extreme device widths: (a) device width equal to 25 μm and (b) device width equal to 75 μm, for all gate fingers biased to conduct a drain current (I_{ds}) of 100 mA/mm across the entire discussed frequency spectrum

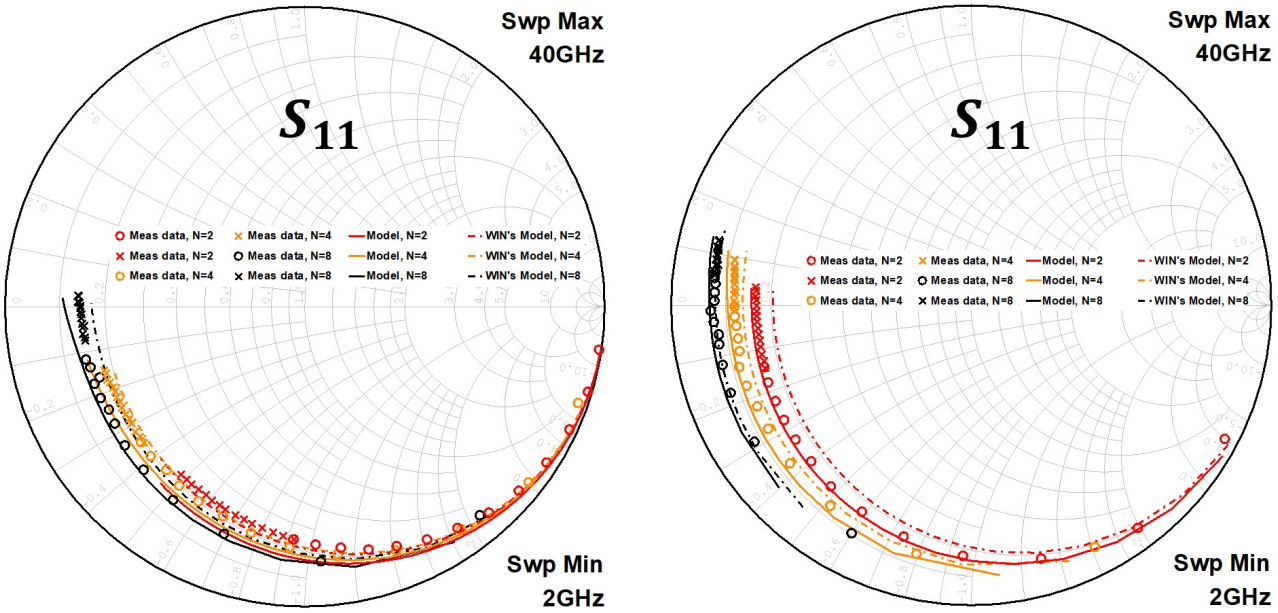

Figure 4.13: A comparison between the measured (in circles and crosses) and analytically obtained S_{11} from our model (in solid lines) and WIN's model (in broken lines) over the two extreme device widths: (a) device width equal to 25 μm and (b) device width equal to 75 μm, for all gate fingers biased to conduct a drain current (I_{ds}) of 100 mA/mm across the entire discussed frequency spectrum

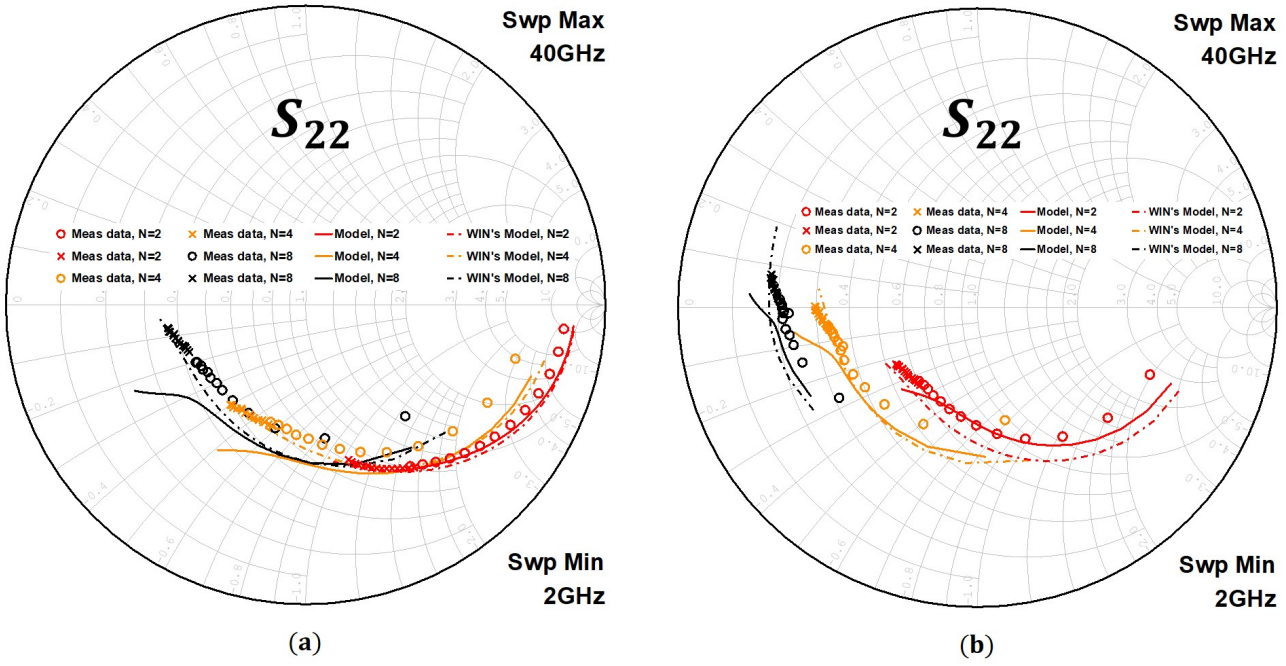

Figure 4.14: A comparison between the measured (in circles and crosses) and analytically obtained S_{22} from our model (in solid lines) and WIN's model (in broken lines) over the two extreme device widths: (a) device width equal to 25 μm and (b) device width equal to 75 μm, for all gate fingers biased to conduct a drain current (I_{ds}) of 100 mA/mm across the entire discussed frequency spectrum

Chapter 5

Conclusion and Future work

The advancement in HEMT technology to cater for high-speed applications has transformed the motion of a charge carrier to be almost ballistic especially in advanced technologies [34–36]. With such a high velocity the time taken by the carriers to cross the channel of the FET has drastically reduced, which makes them almost immune to lattice scattering. Hence, the origin of channel-noise could not be considered as thermal. Instead, the principle of uncertainty, in pointing to both momentum and position of the charge carriers in the channel simultaneously, must be used to model the channel-noise current. As described in Chapter 3, the randomness in the number of charge carriers can be described using probability theory. One such example is Schottky's theorem, that was able to predict the randomness in the total number of thermionic emitted electrons from a cathode.

5.1 Conclusion

As shown in Chapter 3 (in Figure 3.5), correlated noise sources are not sufficient to predict the high-frequency noise performance of the device. We also validated that (as shown in Figure 3.8), both gate and channel noise current are not completely correlated to each other but instead are partially correlated. Furthermore, the contribution of the number of charge carriers inside the buffer layers or in the doped layer in generating a noise current between drain and source terminals cannot be neglected. Since the origin of the noise in the buffer layer is somewhat different from that in the channel, the two noise currents are partially correlated to each other. Thus, in total, three partially correlated noise sources are needed to correctly predict the noise performance of the HEMT over the frequency range of 2 GHz to 40 GHz.

Equations (4.27)-(4.29), written in Verilog-A language, are used to model the contribution of all the three noise sources and the complete model is described in appendix A . There are five model parameters which are needed to define the noise phenomenon in an HEMT. These parameters are functions of the drain current and device width and can be obtained from the response of the noise parameters as discussed in Section 4.4. Hence, a scalable non-linear noise model can be developed

using these equations. The analytically obtained noise parameters using the model are in good agreement with the measured data over various device geometries and bias points, as shown in Figures 4.3 - 4.6. The model was appended into the existing scalable non-linear model for the HEMT [45], and the combined model can predict both noise and other operations of the HEMT as shown in Figures 4.11 - 4.14.

5.2 Future Work

In this work, the noise phenomenon in the HEMT is analysed for the frequency range of 2 GHz to 40 GHz. Therefore, only those noise sources that can affect the performance of the HEMT in this frequency regime are modelled. There are other noise sources such as flicker noise and shot noise that can influence the noise performance of the HEMT in the lower frequency range. The nature of their impact and the influenced frequency range will be studied in future. Also, since the measured data were only limited to a few bias points and device geometries and the high-frequency measured sets have an additional offset, more measurement results are needed to decide on the correct value of γ_{SD} and the average charge in the buffer or in the doped layer, $\overline{q_{blu}}$ and $\overline{q_{blc}}$, respectively. Moreover, apart from normal operation of the device, in many applications the device is subjected to an input pulsed signal. Such pulsed signals can produce generation and recombination noise. The impact of such noise sources on the device behaviour is a challenging task. Relevant literature does exist on the above-discussed three noise mechanisms; flicker noise, shot noise and generation and recombination noise, hence with the help of good noise measurement set-ups these noise sources can be modelled to develop a complete noise model for the HEMT.

Appendix A

Verilog-A Implementation of the Noise Model

The following Verilog-A Module: noise_model() takes the drain current (ids) of the FET as an argument to add the corresponding drain and gate noise currents in the electrical terminals (g,d,s) of the FET.

```
module noise_model (g,d,s,ids);
inout g,d,s;
electrical g,d,s;
‘define P_Q 1.6e-19;
parameter real NFLAG    = 1.0  from [0:1];
parameter real NCW      = 1.0  from [0:1];
parameter real FDS      = 1.0  from [0:100];
parameter real FDSU     = 1.0  from [0:100];
parameter real fcc      = 1.0  from [0:10];
parameter real fblu     = 1.0  from [0:10];
parameter real fblc     = 1.0  from [0:10];
parameter real gammaSD  = 0.5  from [0:1];
real sigma_cor, sigma_uncor, sigma_blu, sqid;
real Noise_GS_Charge, Noise_GD_Charge, Noise_BLU_Charge, Noise_BLC_Charge;
analog begin
     sigma_cor        = white_noise(NFLAG*2*P_Q, "thermal");
     sigma_uncor      = white_noise(NFLAG*2*P_Q, "thermal");
     sigma_blu        = white_noise(NFLAG*2*P_Q, "thermal");
     sqid             = sqrt(ids);

     Noise_GS_Charge  = sigma_cor*sqrt(fcc*gammaSD*P_Q*1e-9*sqrt(ids/1e-3*NCW/25) );
     Noise_GD_Charge  = sigma_cor*sqrt(fcc*(1-gammaSD)*P_Q*1e-9*sqrt(ids/1e-3*NCW/25) );
```

```
    Noise_BLU_Charge = sigma_blu*sqrt(fblu*P_Q*1e-9*sqrt(25/NCW)*(ids/1e-3) );
    Noise_BLC_Charge = sigma_cor*sqrt(fblc*P_Q*1e-9*pow(25/NCW,0.75)*(ids/1e-3) );
    Noise_BLC_Charge = Noise_BLC_Charge +
                       sigma_uncor*sqrt(fblc*P_Q*1e-9*pow(25/NCW,0.75)*(ids/1e-3) );

    I(d,s) <+ sigma_cor*sqrt(1e-2*FDS*pow(1e-3/ids,0.25) )*sqid;
    I(d,s) <+ sigma_uncor*sqrt(1e-2*FDSU*(25/NCW)*pow(ids/1e-3,1.25) )*sqid;
    I(d,s) <+ ddt(Noise_BLU_Charge) + ddt(Noise_BLC_Charge);
    I(g,s) <+ ddt(Noise_GS_Charge);
    I(g,d) <+ ddt(Noise_GD_Charge);
end
endmodule
```

References

[1] A. V. Der Ziel, "Thermal Noise in Field-Effect Transistors," *Proceedings of the IRE*, vol. 50, no. 8, pp. 1808–1812, Aug. 1962.

[2] B. Carnez, A. Cappy, R. Fauquembergue, E. Constant, and G. Salmer, "Noise modeling in submicrometer-gate FET's," *IEEE Transactions on Electron Devices*, vol. 28, no. 7, pp. 784–789, July 1981.

[3] A. V. Der Ziel, "Gate noise in field effect transistors at moderately high frequencies," *Proceedings of the IEEE*, vol. 51, no. 3, pp. 461–467, March 1963.

[4] R. Pucel, H. A. Haus, and H. Statz, "Signal and Noise Properties of Gallium Arsenide Microwave Field-Effect Transistors," *Advances in Electronics and Electron Physics*, vol. 38, pp. 195–265, Dec. 1975.

[5] A. Cappy, "Noise modeling and measurement techniques (HEMTs)," *IEEE Transactions on Microwave Theory and Techniques*, vol. 36, no. 1, pp. 1–10, Jan. 1988.

[6] M. W. Pospieszalski, "Modeling of noise parameters of MESFETs and MODFETs and their frequency and temperature dependence," in *IEEE MTT-S International Microwave Symposium Digest*, vol. 1, June 1989, pp. 385–388.

[7] M. W. Pospieszalski, "On the dependence of FET noise model parameters on ambient temperature," in *2017 IEEE Radio and Wireless Symposium (RWS)*, Jan. 2017, pp. 159–161.

[8] F. Danneville, G. Dambrine, H. Happy, and A. Cappy, "Influence of the gate leakage current on the noise performance of MESFETs and MODFETs," in *1993 IEEE MTT-S International Microwave Symposium Digest*, vol. 1, June 1993, pp. 373–376.

[9] F. Danneville, "Microwave Noise and FET Devices," *IEEE Microwave Magazine*, vol. 11, no. 6, pp. 53–60, Oct. 2010.

[10] A. V. Der Ziel, *Noise in solid state devices and circuits*. New York : Wiley, 1986, a Wiley-Interscience publication. [Online]. Available: https://trove.nla.gov.au/work/18261062

[11] H. Rothe and W. Dahlke, "Theory of Noisy Fourpoles," *Proceedings of the IRE*, vol. 44, no. 6, pp. 811–818, June 1956.

[12] A. E. Parker and S. J. Mahon, "Robust Extraction of Access Elements for Broadband Small-signal FET Models," in *2007 IEEE/MTT-S International Microwave Symposium*, June 2007, pp. 783–786.

[13] G. Dambrine, A. Cappy, F. Heliodore, and E. Playez, "A new method for determining the FET small-signal equivalent circuit," *IEEE Transactions on Microwave Theory and Techniques*, vol. 36, no. 7, pp. 1151–1159, July 1988.

[14] M. Berroth and R. Bosch, "Broad-band determination of the FET small-signal equivalent circuit," *IEEE Transactions on Microwave Theory and Techniques*, vol. 38, no. 7, pp. 891–895, July 1990.

[15] P. M. White and R. M. Healy, "Improved equivalent circuit for determination of MESFET and HEMT parasitic capacitances from "Coldfet" measurements," *IEEE Microwave and Guided Wave Letters*, vol. 3, no. 12, pp. 453–454, Dec. 1993.

[16] R. Anholt and S. Swirhun, "Equivalent-circuit parameter extraction for cold GaAs MESFET's," *IEEE Transactions on Microwave Theory and Techniques*, vol. 39, no. 7, pp. 1243–1247, July 1991.

[17] C. F. Campbell and S. A. Brown, "An analytic method to determine GaAs FET parasitic inductances and drain resistance under active bias conditions," *IEEE Transactions on Microwave Theory and Techniques*, vol. 49, no. 7, pp. 1241–1247, July 2001.

[18] A. Parker, "Getting to the heart of the matter: considerations for large-signal modeling of microwave field-effect transistors," *IEEE Microwave Magazine*, vol. 16, no. 3, pp. 76–86, April 2015.

[19] W. C. Bruncke and A. V. Der Ziel, "Thermal noise in junction-gate field-effect transistors," *IEEE Transactions on Electron Devices*, vol. ED-13, no. 3, pp. 323–329, March 1966.

[20] A. Cappy, A. Vanoverschelde, M. Schortgen, C. Versnaeyen, and G. Salmer, "Noise modeling in submicrometer-gate two-dimensional electron-gas field-effect transistors," *IEEE Transactions on Electron Devices*, vol. 32, no. 12, pp. 2787–2796, Dec. 1985.

[21] H. Fukui, "Optimal noise figure of microwave GaAs MESFET's," *IEEE Transactions on Electron Devices*, vol. 26, no. 7, pp. 1032–1037, July 1979.

[22] M. W. Pospieszalski, "On Certain Noise Properties of Field-Effect and Bipolar Transistors," in *2006 International Conference on Microwaves, Radar Wireless Communications*, May 2006, pp. 1127–1130.

[23] M. W. Pospieszalski and A. C. Niedzwiecki, "FET noise model and on-wafer measurement of noise parameters," in *1991 IEEE MTT-S International Microwave Symposium Digest*, vol. 3, July 1991, pp. 1117–1120.

[24] M. W. Pospieszalski, "Interpreting Transistor Noise," *IEEE Microwave Magazine*, vol. 11, no. 6, pp. 61–69, Oct. 2010.

[25] M. S. Gupta and P. T. Greiling, "Microwave noise characterization of GaAs MESFET's: determination of extrinsic noise parameters," *IEEE Transactions on Microwave Theory and Techniques*, vol. 36, no. 4, pp. 745–751, April 1988.

[26] M. Rudolph, R. Doerner, E. Ngnintendem, and W. Heinrich, "Noise modeling of GaN HEMT devices," in *2012 7th European Microwave Integrated Circuit Conference*, Oct. 2012, pp. 159–162.

[27] M. Rudolph and R. Doerner, "Bias-Dependent Pospieszalski Noise Model for GaN HEMT Devices," in *GeMiC 2014; German Microwave Conference*, March 2014, pp. 1–4.

[28] P. Heymann, M. Rudolph, H. Prinzler, R. Doerner, L. Klapproth, and G. Bock, "Experimental evaluation of microwave field-effect-transistor noise models," *IEEE Transactions on Microwave Theory and Techniques*, vol. 47, no. 2, pp. 156–163, Feb. 1999.

[29] Y. Chang, S. Lin, H. Chiou, D. Chang, and Y. Juang, "On-wafer noise figure measurements of millimeter-wave LNA and mixer," in *2010 Asia-Pacific Microwave Conference*, Dec. 2010, pp. 1424–1427.

[30] K. Shinohara, Y. Yamashita, A. Endoh, K. Hikosaka, T. Matsui, T. Mimura, and S. Hiyamizu, "Extremely High-Speed Lattice-Matched InGaAs/InAlAs High Electron Mobility Transistors with 472 GHz Cutoff Frequency," *Japanese Journal of Applied Physics*, vol. 41, pp. 451–454, April 2002.

[31] C. Kuo, H. Hsu, E. Y. Chang, C. Chang, Y. Miyamoto, S. Datta, M. Radosavljevic, G. Huang, and C. Lee, "RF and Logic Performance Improvement of $In_{0.7}Ga_{0.3}As/InAs/In_{0.7}Ga_{0.3}As$ Composite-Channel HEMT Using Gate-Sinking Technology," *IEEE Electron Device Letters*, vol. 29, no. 4, pp. 290–293, April 2008.

[32] J. Millán, P. Godignon, X. Perpiñà, A. Pérez-Tomás, and J. Rebollo, "A Survey of Wide Bandgap Power Semiconductor Devices," *IEEE Transactions on Power Electronics*, vol. 29, no. 5, pp. 2155–2163, May 2014.

[33] M. Barsky, M. Biedenbender, X. Mei, P. Liu, and R. Lai, "Advanced InP and GaAs HEMT MMIC technologies for MMW commercial products," in *2007 65th Annual Device Research Conference*, June 2007, pp. 147–148.

[34] Y. Awano, K. Tomizawa, N. Hashizume, M. Kawashima, and T. Kanayama, "Performance and principle of operation of GaAs ballistic FET," vol. 29, Feb. 1983, pp. 617–620.

[35] Y. Awano, M. Kosugi, T. Mimura, and M. Abe, "Performance of a quarter-micrometer-gate ballistic electron HEMT," *IEEE Electron Device Letters*, vol. 8, no. 10, pp. 451–453, Oct. 1987.

[36] Y. Awano, M. Kosugi, S. Kuroda, T. Mimura, and M. Abe, "Electron dynamics and device physics of short-channel HEMTs: transverse-domain formation, velocity overshoot, and short-channel effects," in *Proceedings., IEEE/Cornell Conference on Advanced Concepts in High Speed Semiconductor Devices and Circuits*, Aug. 1989, pp. 46–55.

[37] N. Wiener, "Generalized harmonic analysis," *Acta Math.*, vol. 55, pp. 117–258, 1930. [Online]. Available: https://doi.org/10.1007/BF02546511

[38] A. E. Parker and S. J. Mahon, "Charge partitioning scheme for FET models," in *2014 9th European Microwave Integrated Circuit Conference*, Oct. 2014, pp. 237–240.

[39] G. J. Coram, "How to (and how not to) write a compact model in Verilog-A," in *Proceedings of the 2004 IEEE International Behavioral Modeling and Simulation Conference, 2004. BMAS 2004.*, Oct. 2004, pp. 97–106.

[40] C. McAndrew, G. Coram, A. Blaum, and O. Pilloud, "Correlated noise modeling and simulation," in *Proc. Tech. Workshop Compact Modeling*, 2005, pp. 40–45.

[41] P. M. Smith, P. C. Chao, K. H. G. Dub, L. F. Lester, B. R. Lee, and J. M. Ballingall, "Advances in HEMT Technology and Applications," in *1987 IEEE MTT-S International Microwave Symposium Digest*, vol. 2, May 1987, pp. 749–752.

[42] S. Lawrence Selvaraj, T. Suzue, and T. Egawa, "Breakdown Enhancement of AlGaN/GaN HEMTs on 4-in Silicon by Improving the GaN Quality on Thick Buffer Layers," *IEEE Electron Device Letters*, vol. 30, no. 6, pp. 587–589, June 2009.

[43] Y. C. Choi, M. Pophristic, H. Cha, B. Peres, M. G. Spencer, and L. F. Eastman, "The Effect of an Fe-doped GaN Buffer on off-State Breakdown Characteristics in AlGaN/GaN HEMTs on Si Substrate," *IEEE Transactions on Electron Devices*, vol. 53, no. 12, pp. 2926–2931, Dec. 2006.

[44] C. Poblenz, P. Waltereit, S. Rajan, S. Heikman, U. K. Mishra, and J. S. Speck, "Effect of carbon doping on buffer leakage in AlGaN/GaN high electron mobility transistors," *Journal of Vacuum Science & Technology B: Microelectronics and Nanometer Structures Processing, Measurement, and Phenomena*, vol. 22, no. 3, pp. 1145–1149, 2004.

[45] A. E. Parker, "Advances in nonlinear characterization of millimetre-wave devices for telecommunications," vol. 6798, Dec. 2007. [Online]. Available: https://doi.org/10.1117/12.759297